From Solid Surfactants to Micromotors: An Overview of the Synthesis and Applications of Heterogeneous Particles

Alex McGlasson[1] and Thomas P. Russell[1,2]*

[1]Department of Polymer Science and Engineering, University of Massachusetts Amherst, Amherst, Massachusetts, 01003, United States

[2]Material Science Division, Lawrence Berkeley National Laboratory, Berkeley, CA, 94720, United States

*Corresponding Author's Email: russell@mail.pse.umass.edu

Abstract

Colloid science has classically concerned itself with the investigation of the properties of dispersed phases in a bulk medium. This has led to the development of a rich amount of chemistry, physics, and engineering that have facilitated the evolution and maturation of this field. One of the many developments made over the last 30 years is the introduction of particles that are heterogeneous in chemistry and shape. These heterogeneities can introduce behaviors that are not achievable in homogeneous systems and that are specific to the type and class of nonuniformity. This has led to the development of numerous technologies, two of which are Janus micromotors and solid surfactants. This review aims to familiarize the reader with the field of heterogeneous particles. We begin with an overview of various synthetic methods to produce colloidal particles that are heterogeneous in chemistry and shape. We then discuss their use as solid surfactants and autonomous micromotors, and then summarize and provide a future perspective on the field.

Introduction

A colloid is very broadly defined as a material that is finely dispersed in second where the resultant properties of the dispersion are different than that of the two bulk phases [1,2]. This classic definition of a colloid is purposefully broad to encompass multiple systems. The four main classes of colloids that arise from this broad definition are then sols, emulsions, foams, and aerosols (Figure 1). A sol is a dispersion of solid particles in a liquid medium [3,4]. In modern definitions of the term colloids or colloidal solutions, the authors are most-often referring to sols or the particles dispersed in sols. A few examples of sols are polystyrene or silica microspheres that are dispersed in aqueous or organic solutions. Dispersions of liquid droplets in a second liquid medium are known as emulsions [5,6]. Emulsions typically are droplets of an oil phase dispersed in an aqueous media or vice versa. These droplets are then stabilized using a variety of surfactants or solid particles. This makes emulsion droplets particularly useful since this enables the transport or dispersion of materials in a medium in which it is not soluble. Like emulsions and sols, a foam is a dispersion of gaseous bubbles in a solid or liquid medium [7–9]. Introducing the gaseous bubbles significantly reduces the density of the material to yield lightweight materials with unique engineering properties. An aerosol is a dispersion of solid or liquid particles in a gaseous medium [10,11]. Each of these classes of colloids has been researched by many groups and thoroughly reviewed by other authors. In this review we will focus on sols in which the solid particles in the sol contain a built-in heterogeneity.

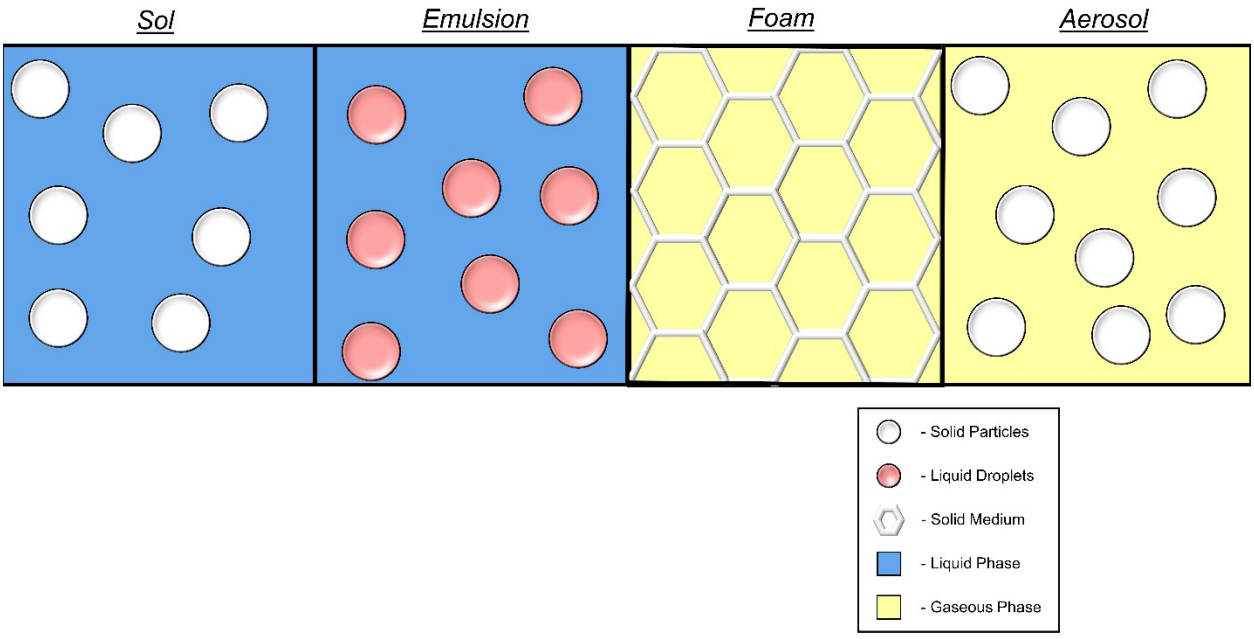

Fig. 1 – A schematic depicting the various classes of colloids.

Research into sols containing solid heterogeneous particles garnered significant interest in the 1990s after de Gennes first coined the term Janus particle in his 1991 Nobel Prize lecture [12]. He hypothesized that particles containing two chemically dissimilar faces have the potential to more efficiently stabilize interfaces compared to small-molecule surfactants. This birthed the idea of using Janus particles as solid surfactants, which are colloidal particles that readily assemble at and stabilize the interface between immiscible fluids. The idea of using colloidal particles as solid surfactants was not a new one [13–16]. However, the production and synthesis of colloidal surfactants often focused on how to create narrowly dispersed spherical particles. Since the initial formulation of the concept of a Janus particle, heterogeneous particle synthesis has branched off to focus on two types of heterogeneities. The first is chemical heterogeneity, as proposed by de Gennes, where the particle is chemically heterogeneous. The second is morphological heterogeneity, where the particle shape is not necessarily spherical and contains a shape anisotropy.

To describe the various classes of particle heterogeneities, a seemingly infinite number of possible descriptions of particle morphologies has emerged. However, there are several common

morphologies which we will classify (Figure 2). Janus particles, one of the most ubiquitous and simplest classes of heterogeneous colloids, are particles with two chemically dissimilar hemispheres [17–23]. A common example is an amphiphilic Janus particle where one half of the particle is hydrophobic, and the other half of the particle is hydrophilic [24,25]. Recent literature has also placed additional emphasis on the synthesis of Janus particles in which the materials are sustainable or have a biological origin [26–28]. Similar to Janus particles are patchy particles [29–33]. Patchy particles are similarly chemically heterogeneous, but the heterogeneities are distributed over the surface of the particle. The patches can vary in size and shape depending on the synthesis and processing used to make the particles.

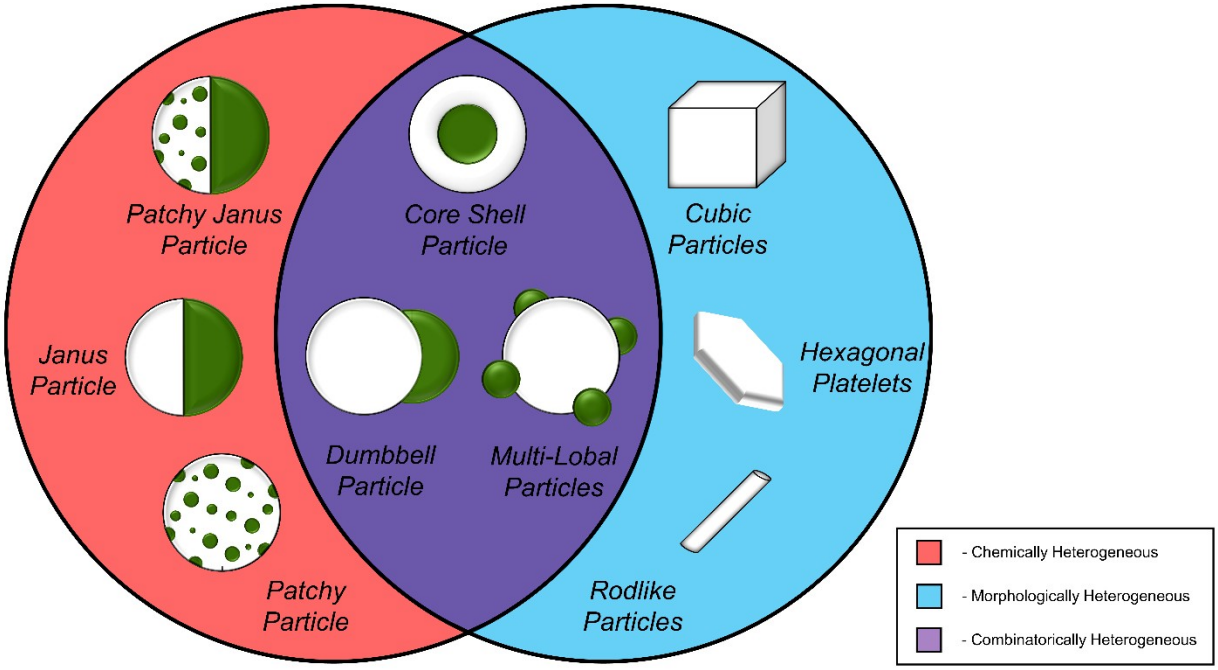

Fig. 2 – A schematic diagram depicting some selected examples of chemically, morphologically, and combinatorically heterogeneous particles.

There are also many varieties of morphologically heterogeneous particles. Advances in synthesis have enabled the synthesis of non-spherical particles of a regular shape (e.g., rods, cubes, and hexagonal platelets) [34–40]. In addition, there have been significant advances in producing particles with more irregular and unique morphologies [28,34,41–44]. Some examples include patchy Janus particles [45–47], dumbbell particles [48–54], multi-lobal particles [55–60], or core-shell particles [61–66]. The variety and uniqueness of the different shapes illustrates the

high degree of control that has been developed, enabling the synthesis of many unique varieties of heterogeneous particles that can be used for various applications. This makes the term heterogeneous particles itself an incredibly broad term that includes many classes of particles. However, for this review we will focus on Janus or Janus-like heterogeneous particles since these particles have been popular in recent literature.

In this review we will first discuss some popular synthetic techniques for producing chemically or morphologically heterogeneous particles and some selected applications. The specific synthetic techniques discussed will be self-assembly and physical vapor deposition, Pickering emulsion masking, and seeded emulsion polymerization. We will then discuss some specific applications of heterogeneous particles, including the assembly of particles at fluid interfaces and their use as autonomous micromotors.

Synthesis of Heterogeneous Particles

Self-Assembly and Physical Vapor Deposition

Self-assembly coupled with physical vapor deposition is one of the more straightforward techniques for the fabrication of Janus particles (Figure 3a). As the name suggests, this method begins with self-assembling a monolayer or sub-monolayer of pre-synthesized solid particles on a planar substrate. Post-assembly, a metallic or inorganic oxide layer is deposited onto the particles using physical vapor deposition (PVD). The assembly of the particles onto the 2D substrate and the directionality of the stream of metal atoms showering down on the assembly masks one half of the particle. This allows only one half of the particles to be coated with the metal, generating the Janus configuration. This technique is used to produce Janus particles where one domain is the solid particle phase and the other is a noble metal or an inorganic oxide. This technique became popular and remains one of the most popular techniques due to its simplicity. Additionally, the only specialized laboratory equipment needed to produce Janus particles by this method is a PVD system.

Figure 2 – Figure depicting PVD and different results taken from others

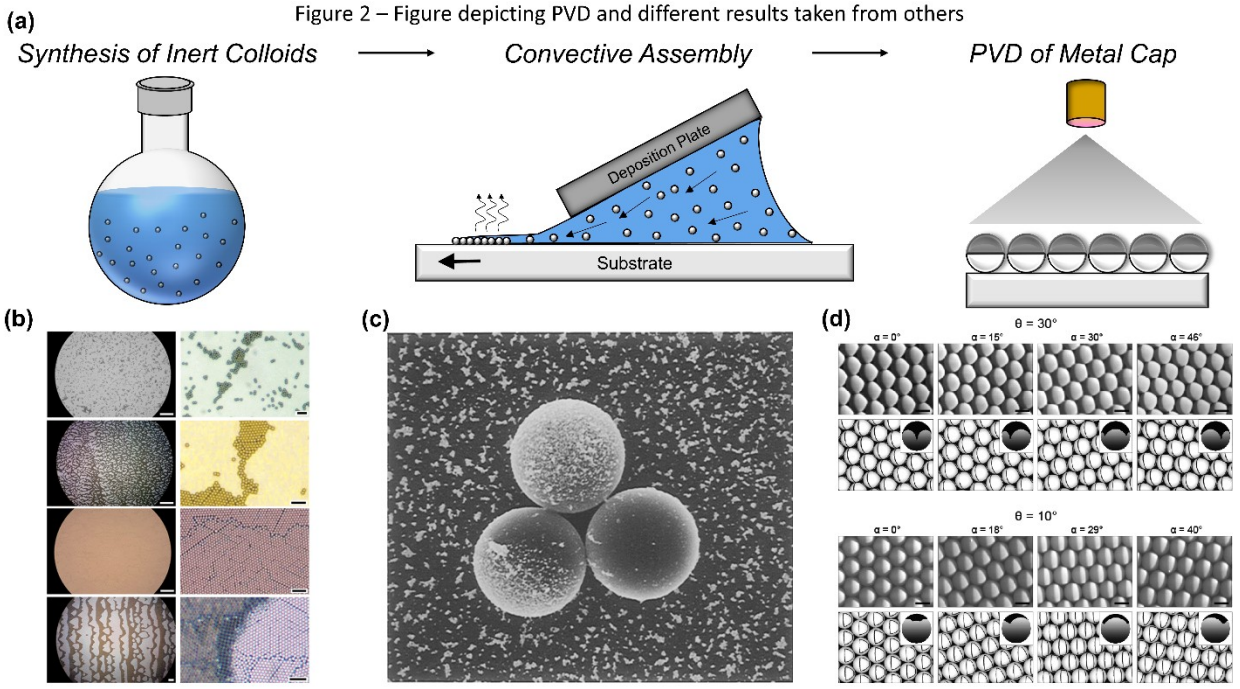

Fig. 3 – (a) A schematic diagram illustrating the self-assembly and physical vapor deposition technique. Reproduced with permission [67]. Copyright 2021, Wiley-VCH. This first begins with the synthesis of Inert colloids which are then convectively assembled into (b) monolayer or sub-monolayer configurations. Reproduced with permission. Copyright 2004, The American Chemical Society. One can then perform (c) PVD to obtain Janus particles or (d) GLAD at various angles to obtain patchy particles. Reproduced with permission [33,68]. Copyright 1997 and 2008, The American Chemical Society.

In the first step of this fabrication process, one must either synthesize or purchase the base particle system. With the advancement of synthetic processes there are a wide number of methods and suppliers through which one can either synthesize or purchase the base particle. Two common choices for the base particles are polystyrene and silica colloids of a wide range of sizes and surface chemistries. To synthesize polystyrene colloids, heterogeneous polymerization techniques, such as emulsion or dispersion polymerization, are commonly used. These and other heterogeneous polymerization techniques have been extensively reviewed by others [69–72]. A commonly utilized technique to produce silica colloids is the Stöber method or a variation of it

[73]. This technique has similarly been extensively reviewed and the reader is directed to them for in depth treatments [74–77].

In the second step of the fabrication process, the particles are convectively assembled into either a monolayer or sub-monolayer configuration using various methods. A technique popularized in the early 2000s was the controlled rapid deposition of particles using blade coating or flow coating [78–80]. Here, a highly concentrated sol is dispensed behind a blade raised slightly above a movable substrate. The substrate is then pulled at a controlled rate so that the evaporating solvent and resulting convective mass transfer causes the particles to assemble in a sub-monolayer, monolayer, or multi-layer configuration (Figure 3b). The resultant morphology of the assembly is a function of multiple variables, including sol concentration, substrate pulling rate, and solvent evaporation rate. Like blade coating, drop casting is where a sol of a known concentration and volume is dispensed onto a planar substrate [81–84]. The solvent of the sol is then evaporated as the particles assemble on the substrate and form assemblies. This is the simplest of all the convective assembly techniques. These techniques and advances in the formation of particle assemblies have been extensively reviewed by other authors [85–89].

The final step of the fabrication process is the PVD of a metallic or inorganic oxide layer to form the Janus morphology (Figure 3c). Two common PVD techniques used to achieve this are sputter coating and evaporative deposition. Sputter coating is a technique in which a target material is bombarded with a high energy plasma or gas under vacuum [90,91]. This causes the ejection of target material in the form of small particulates that bombard and are deposited on the sample. Evaporative deposition is where small noble metal or inorganic ingots are heated to high temperatures in a high vacuum environment [68,92–94]. The high vacuum decreases the boiling point of these materials dramatically allowing the metallic or inorganic material to evaporate and deposit onto the sample substrate. Typically, sputter coating requires a lower vacuum environment but gives less uniform coatings than evaporative deposition while the converse is true. In both sputter coating and evaporative deposition, the separation distance between the sample and the source, along with the lateral dimensions of the sample, define a solid angle. The greater the distance between the sample and the source, the smaller the solid angle will be. This minimizes the divergence of the stream of atoms deposited on your sample and is important for defining the geometry of the resulting coating on the particles. To manipulate this solid angle and

produce patchy particles which do not exhibit a Janus morphology, one can perform what is known as glancing angle deposition (GLAD) (Figure 2d). [29,32,33] By tilting the substrate at controlled angles this facilitates the deposition of controlled patch sizes that do not fully coat the unmasked portion of the assembled particle. GLAD is typically limited for use by thermal evaporation systems and cannot be reliably performed with sputtering systems. This is because sputtering is not a strict line of sight method, unlike thermal evaporation. Sputtering often yields coating beyond the line of sight due to the low-vacuum environment and the mechanism of deposition. Therefore, it is not possible to obtain uniform patch sizes with sputtering systems that one can obtain with thermal evaporation. The final step in the fabrication process is the release of the particles from the deposition substate and dispersion into the final fluid phase. This is usually done via ultrasonication of the substrate in a corresponding fluid phase.

Self-assembly and PVD in addition to being one of the more straightforward techniques for fabricating Janus particles, also comes with several distinct advantages. First, one can consistently create Janus particles with a well-defined and controlled morphology. In addition, the size range of Janus particles that can be synthesized using this technique are only limited by how small or large one can make their base particle. This means that the size of Janus particles obtained from this technique can vary from tens of nanometers all the way to hundreds of microns. In a similar way, particle amphiphilicity and the surface characteristics of one domain can easily be tuned. This can be done via the deposition from a wide range of materials that can be subsequently functionalized using a variety of chemistries, like silane functionalization or Au-thiol chemistry [95–100]. However, the total volume of particles produced by this method is typically small, since one is physically limited by the size of the 2D substrate. In addition, the requirement of various levels of vacuum for both sputtering and evaporation makes this synthesis process highly energy intensive and not scalable. This ultimately limits this technique to use in academic lab settings.

Pickering Emulsion Masking

Like self-assembly and physical vapor deposition, Pickering emulsion masking produces Janus particles by modifying an unmasked portion of a self-assembled chemically homogeneous particle. In Pickering emulsion masking the masking of the particle is done by imbedding the

colloid at an oil/water interface in an oil in water emulsion rather than assembling them on a substrate (Figure 4a). This allows one to modify the exposed surface while the phase imbedded in the oil phase retains the original functionality producing a Janus particle. This technique was originally popularized in the early 2000s and has been used by various groups as a strategy for synthesizing Janus particles [101–104]. This technique continues to remain popular due to the high modularity in chemical functionalities that can be added to the particle surface. In addition, all steps in this process are potentially scalable.

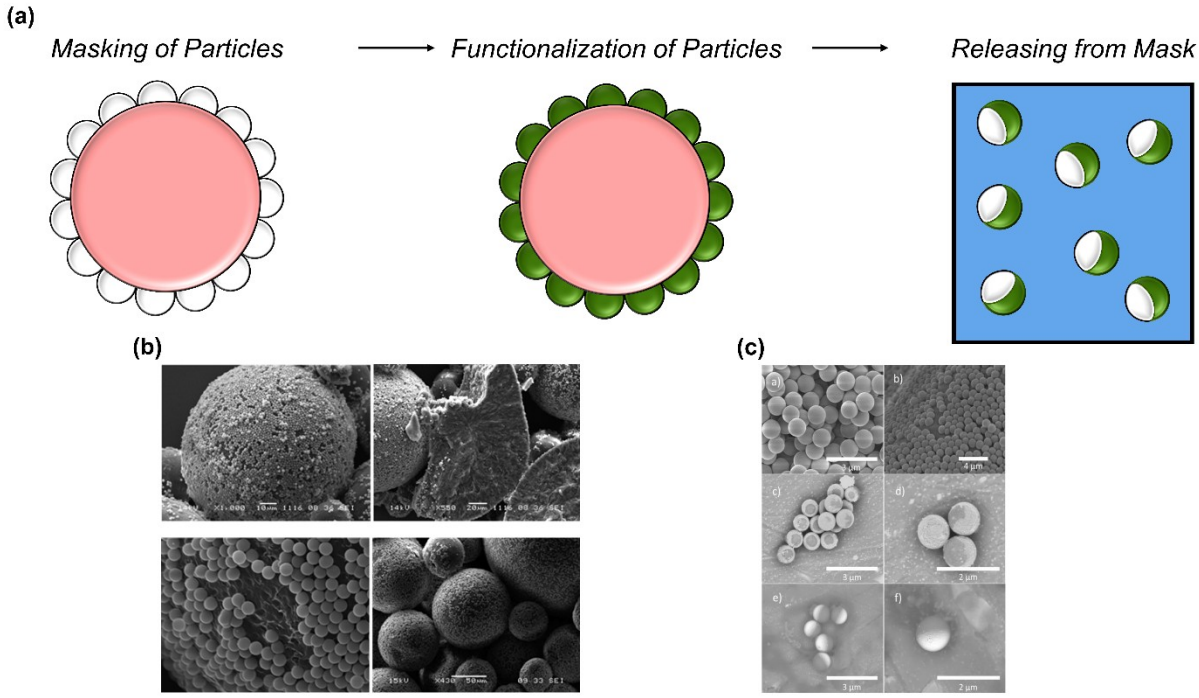

Fig. 4 – (a) A schematic diagram illustrating the Pickering emulsion masking technique. This begins first with the masking of particles in (b) Pickering emulsion droplets where one portion of the particle is exposed. Reproduced with permission [101]. Copyright 2006, The American Chemical Society. These can be (c) functionalized using single step or multi-step functionalization to obtain complex Janus particle structures. Reproduced with permission [105]. Copyright 2017, Wiley-VCH. In the final step the particles are released via dissolution of the wax mask.

This process, like other masking techniques, begins with the choice of the base particle system. The most common choice for a base particle is particles made from silica. There are

several reasons why this is the case. Non-chemically modified silica colloids are inherently hydrophilic making them easy to disperse in water. Large volumes of silica colloids of varying sizes can be synthesized and chemically modified using a combination of a modified Stöber method and silane surface functionalization [97–100]. All these factors combine to make silica particles an ideal candidate for use in Pickering emulsion masking.

After choosing a base particle system, the particles are then dispersed in an aqueous solvent mixture and emulsified with an immiscible oil phase. The aqueous phase typically contains some amount of small-molecule surfactant that assembles at the interface prior to the particle assembly. These surfactants form a monolayer at the interface to reduce the interfacial tension between the oil and water phases. This has the added benefit of changing the charge of the oil-water interface from a negative charge to a positive charge. This promotes the interfacial assembly of the charged particles at the interface by having them interact with the oppositely charged surfactants and anchoring the particles to the interface [106–109]. The concentration of the surfactant in the system enables control of the contact angle of the particles adsorbed to the interface. By tuning the particle contact angle at the interface, the extent to which the particle penetrates the interface, i.e. the immersion depth, can be tuned. This gives precise control of the location of the Janus boundary on the particle and the size of each domain of the Janus particle. The sol is then rapidly mixed with a high melting point oil phase, typically paraffin wax, at a temperature above its melting point [110]. The oil phase chosen should be a solid at room temperature, but its melting point should be below the boiling point of your sol. High melting point oils are used to help prevent the release of the particles from the interface. This ensures the domain imbedded in the oil phase remains masked and is not chemically modified. The rapid and vigorous mixing promotes the formation of the Pickering emulsion droplets and assembles the particles at the oil/water interface (Figure 4b). The solution is then cooled to room temperature, whereupon the oil phase solidifies imbedding the particles at the interface of the emulsion droplet.

After imbedding the particles at the droplet interface, one can then functionalize the exposed portion of the particle. If one is using silica particles, this functionalization step could be as simple as performing a single silane coupling reaction. However, the functionalization of these particles can be complex multistep processes. One can even attach catalytic enzymes or

grow metallic layers on the exposed surface of the particles that are imbedded in the solidified oil phase (Figure 4c) [105,111–113]. The final step in the process is to release the particles from their mask. This usually involves washing the imbedded particles with an organic solvent that will dissolve the wax phase and not affect the modification of the exposed portion of the particle. Upon release from the mask the particles are then usually further washed to ensure the removal of all undesired organics present in the newly formed sol.

Pickering emulsion masking remains a popular technique to produce Janus particles for several reasons. The assortment of silane coupling agents that are commercially available enable the functionalization of the exposed surface of the particles in a variety of ways. Like self-assembly and physical vapor deposition, the size of Janus particles obtained from this technique are only limited by the size of the base particle. This means that the final particle size can similarly range from 10s of nanometers to 10s of microns. The position of the Janus boundary and the percent of the surface functionalization can easily be tuned by tuning the initial surfactant concentration in the aqueous phase. In addition, Pickering emulsion masking does not require the use of specialized laboratory equipment. However, Pickering emulsion masking does have its drawbacks. The number of Janus particles obtained from this technique is still relatively low. This is because the total number of particles that can be converted to Janus particles is limited by the total oil/water interfacial area formed.

Seeded Emulsion Polymerization

Seeded emulsion polymerization is a versatile heterogeneous polymerization technique that can be used to synthesize Janus particles and other heterogeneous polymer particles (Figure 5a) [114]. This is done by swelling a polymeric seed particle with a polymerizable monomer feed in a surfactant stabilized seeded emulsion droplet. The monomer feed can contain either one monomer or multiple monomers, cross-linkers, and an initiator for polymerization. The monomer feed is then polymerized, triggering phase separation within the seeded emulsion droplet. If the polymerized monomer feed is chemically dissimilar to the seed particle, a chemically and morphologically heterogeneous polymer particle results. This technique remains popular since it is an efficient route to produce particles having a wide range of morphologies, chemistries, and sizes in large quantities. Additionally, there is a high degree of tunability in both the final particle

morphology and chemistry. Both of which can be controlled by varying the reaction conditions, monomer feed composition, and seed particle or monomer feed identity.

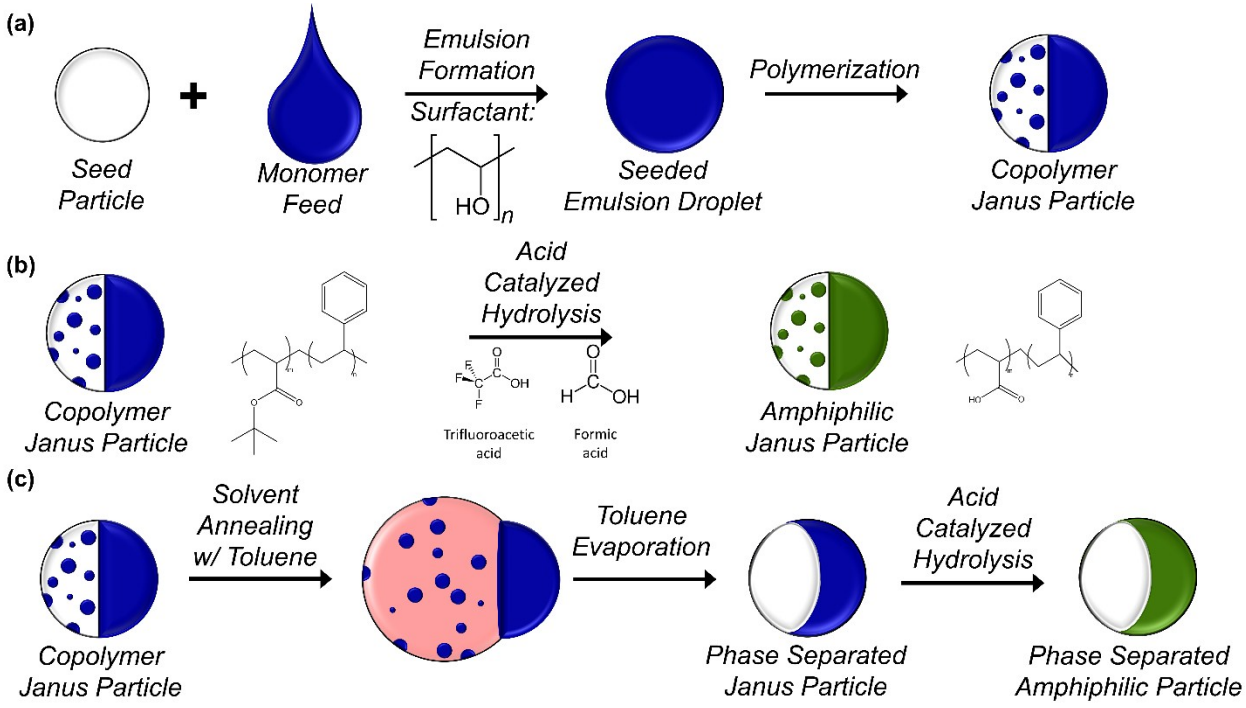

Fig. 5 – (a) A schematic diagram illustrating the seeded emulsion polymerization technique. This begins with the swelling of a chosen seed particle with a monomer feed in a surfactant stabilized seeded emulsion droplet. The monomer feed is then polymerized to obtain a copolymer Janus particle. One can then either (b) chemically functionalize one phase of the particle or (c) morphologically tune the particle. This allows one to simultaneously control the particle chemistry, but also its degree of heterogeneity.

Seeded emulsion polymerization begins with the synthesis of a polymer seed particle using the same heterogeneous polymerization techniques described for the other methods. Heterogeneous polymerization can be leveraged to produce seed particles of a wide range of chemistries and sizes. The initial seed particle can also be cross-linked or uncross-linked. Crosslinking of the seed particle will produce drastically different morphologies upon initiation of the polymerization in the seeded emulsion droplet. Seed particles that are uncross-linked tend to remain spherical and produce particles with phase separated morphologies, like Janus particles [42,45–47]. Seed particles that are crosslinked will begin to expel the swollen monomer feed

upon initiation of polymerization in the seeded emulsion droplet. This tends to produce particles that are either bi-lobal or multi-lobal [57,115,116]. The seed particle can consist of a wide range of different polymers, but a common choice is polystyrene. This is because polystyrene can easily be swollen by many vinyl monomer feeds making it an ideal seed phase.

After the synthesis of the seed particle, the next step is the formation of the seeded emulsion droplet. Typically, these droplets are an oil-in-water emulsion since the polymeric seed particles commonly used are oil soluble polymers. However, water-in-oil emulsion systems with water soluble seed particles and monomer feeds contained within an oil phase can be designed. Contained within the seeded emulsion droplet is an initiator for polymerization, a mixture of monomers, and the swollen polymeric seed particle. The initiators used in seeded emulsion polymerizations are typically thermal radical initiators to perform free radical polymerization of the monomer feed. However, one can also include RAFT or ATRP chain-transfer agents to help control the rate of polymerization and dispersity of the polymerized chains [117–122]. When selecting a monomer or monomers for the monomer feed, one can choose any monomer that is a good solvent for the seed particle polymer. This ensures that the particle is fully swollen inside of the seeded emulsion droplet and there is no initial phase separation occurring within the droplet. One can also choose monomers that can be chemically transformed post synthesis to further alter the chemistry of the particles. Two such examples are incorporating tert-butyl acrylate and propargyl acrylate as part of the monomer feed [45–47]. One can also incorporate a cross-linker into the monomer feed. This is especially desirable when one is attempting to synthesize amphiphilic particles. The hydrophilic domain will become susceptible to dissolution post synthesis, if a crosslinker is not incorporated as part of the monomer feed. The stabilizer used for the seeded emulsion droplet can either be an aqueously soluble polymeric surfactant, like poly(vinyl alcohol), or a small molecule surfactant, like SDS or CTAB. In all cases the identity of the polymeric seed particle, monomer feed, dispersed phase, and emulsion stabilizer will dictate the final morphology of the resulting Particle. Previous authors have shown that the three-phase contact line that results from the immiscible interface of these three liquids is the governing factor for the particle morphology [42,123]. To form biphasic Janus particles, the contact angles of all three phases at the three-phase contact line must be less than 180° but then add to be more than 180°. The two classes of biphasic Janus particles that can form in this way

are concavo-convex and bi-convex Janus particles. In addition to the formation of Janus particles, one can also form core-shell particles by similarly tuning the contact angles at the three-phase contact lines. Therefore, by carefully tuning the system interfacial tensions, one can have a large extent of control over the resulting particle morphology.

Post-formation of the seeded emulsion droplet, one can then initiate the polymerization of the monomer feed. Initially, the seed particle is soluble in the monomer feed and will continue to be soluble in the early stages of polymerization. As the monomer feed polymerizes and increases in molecular weight, the seed and the growing polymer will phase separate. This idea of using polymeric phase separation to produce Janus particles is not unique to seeded emulsion polymerization. Several other authors have utilized phase separation of block-copolymers to produce Janus particles and other heterogeneous particles [124–130]. In some cases, these systems produce particles with unique morphologies that are only possible through the microphase separation of block-copolymers [131–135]. In the case of seeded emulsion polymerization, phase separation that causes the formation of a Janus-like particle has been termed homopolymer or copolymer induced phase separation [47]. Polymerization and phase separation will continue until the monomer feed is exhausted or the glass transition temperature of either phase increases above room temperature arresting phase separation due to a reduction in mobility. Consequently, a kinetically trapped morphology is produced with particles having interpenetrating patches of one domain (Figure 6a). This can be avoided if one includes a small amount of good solvent for both phases inside of the seeded emulsion droplet that keeps the glass-transition temperature depressed. This allows the phase separation to continue to the point of obtains a biphasic morphology (Figure 6b) [42]. Incorporating this solvent into the monomer feed allows the phases to stay mobile towards the end of the polymerization and allows for complete phase separation.

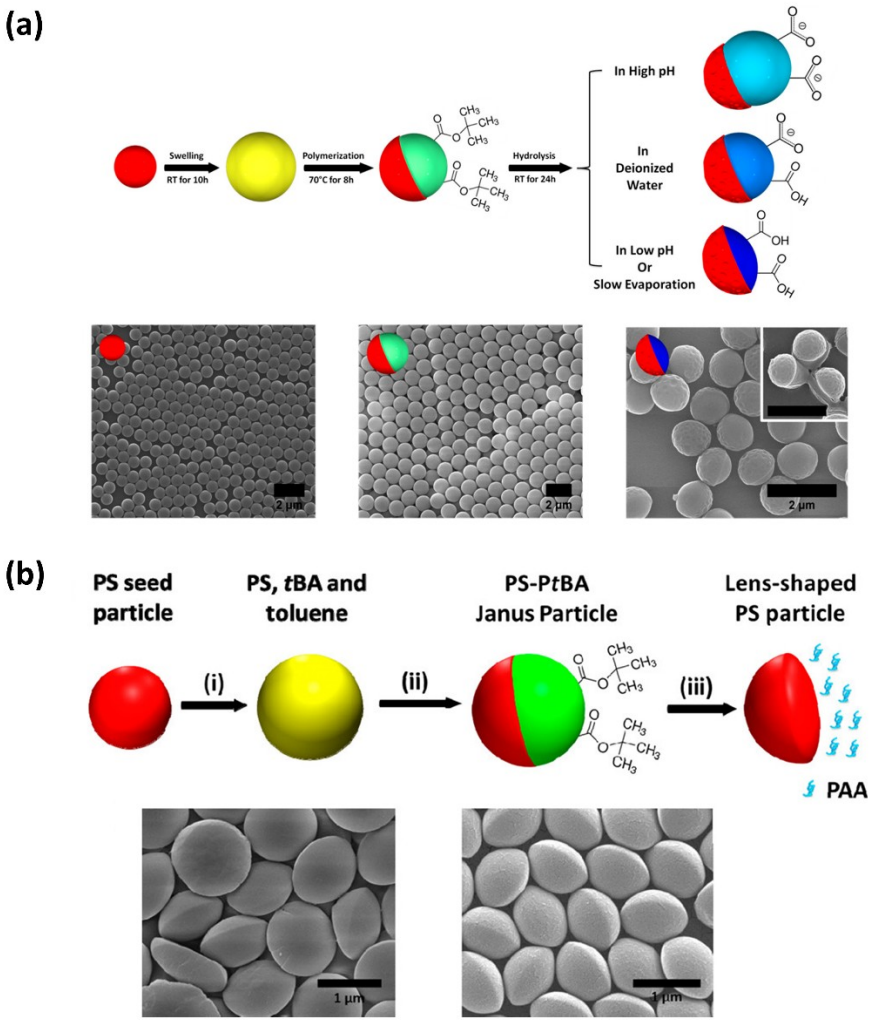

Fig. 6 – Examples of SEP syntheses which yield (a) Patchy Janus particles and (b) lens shaped particles by tuning the composition of the monomer feed. Reproduced with permission [42,46]. Copyright 2014 and 2017, The American Chemical Society.

Post-synthesis one can subsequently tune both the chemical composition and the morphology of the synthesized particles. This can be done by performing a functionalization reaction that chemically transforms either the polymerized monomer feed or the seed particle domain. One such example is the previously discussed synthesis of heterogeneous polymer particles by polymerizing a monomer feed composed of styrene and tert-butyl acrylate swollen inside of a polystyrene seed. Post polymerization, the tert-butyl acrylate can be converted to poly(acrylic acid) using an acid catalyzed hydrolysis (Figure 5b). If the monomer feed phase is

crosslinked, this will result in a highly amphiphilic Janus particle that is pH responsive. If the monomer feed phase is not crosslinked, this will enable the sacrificial dissolution of the monomer feed phase to yield particles with unique morphologies, like porous bowls and golf balls [47]. To tune the morphology of the particle one can perform a process known as solvent assisted phase separation (Figure 5c). Here, the synthesized particle is swollen with a good solvent inside of a surfactant stabilized droplet. The domains are then allowed to phase separate and coarsen. After annealing, the solvent is evaporated, and one obtains particles with the coarsened phase separated morphology [47]. The final morphology obtained from this process will be a function of the three-phase contact line between the solvent, the swollen polymer, and the surrounding solvent media [42,123]. Therefore, one could tune the morphology simply by changing both the annealing solvent and the surfactant species. Using a combination of these techniques one can morphologically and chemically tune their initially synthesized particles.

Seeded emulsion polymerization has the unique advantage over other methods for producing heterogeneous colloids in that it can produce particles with more unique morphologies. Self-assembly combined with PVD and Pickering emulsion masking are strategies limited to producing particles with only Janus and patchy morphologies. The size of the resulting particles is typically limited by the initial size of the seed particle, which can range from 10s of nanometers to several microns. In addition, particles that result from SEP can easily be chemically and morphologically tuned. Seeded emulsion polymerization is also scalable and can be used to produce large quantities of heterogeneous particles. However, particles made with seeded emulsion polymerization can only be made of polymeric materials. Additionally, this method may also require significant synthetic optimization to obtain the desired morphology and chemistry.

Applications of Heterogeneous Particles

Assembly at Fluid Interfaces

When two immiscible fluids are brought into contact there is a thermodynamic energy penalty that must be paid by the system to allow for the formation of an interface [136–138]. The amount of energy required to form an interface is known as the interfacial energy between the two fluids. Immiscible systems will inherently attempt to minimize the thermodynamic energy

penalty to form an interface. This minimization can be accomplished in a variety of ways. The most common way is to reduce the total interfacial area by coarsening the phases. This tendency for the interface to shrink to the minimum surface area possible is captured through the interfacial tension. The interfacial tension is defined as the amount of thermodynamic work that must be expended to form a new interface with a given interfacial area. Regardless of the number of components or the number of phases, interfacial area and surface area will always be minimized assuming no constraints. A planar interface between two fluids or a flat surface for a liquid represent the equilibrium, lowest energy state.

Another means to reduce the interfacial energy is to adsorb particulates or other molecules to the interface. If the interaction energy between the two fluids is greater than the sum of the interaction energies of the fluids with the particles, adsorption of the particles will occur. The materials that adsorb the interface and decrease the interfacial tension between two liquids are known as surface active agents or surfactants. Surfactants can be small molecules, nanoparticles, or colloidal particles. Small molecule surfactants are widely used in many applications and have been extensively studied and treated in numerous review articles and books [139–142]. It was first discovered in the pioneering work of Ramsden [143] and Pickering [144] that particles and other macromolecules could be used as surfactant materials. Their work showed that colloidal particles or other nanomaterials dispersed in either phase will readily segregate to a fluid interface to reduce the interfacial tension. Emulsions that are formed with colloidal particles or other nanomaterials rather than small molecule surfactants are now known as Pickering emulsions [145–155]. Pickering emulsions are often utilized over traditional small molecule surfactants due to their resistance to coalescence and enhanced emulsion stability.

The energy reduction that occurs from the adsorption of colloidal particles to interfaces was first computed by Koretsky and Kruglyakov [106,156]. For spherical particles with a homogenous surface chemistry the reduction in interfacial energy is found to be,

$$\Delta E = \pi r^2 \gamma_{ow} \left(1 - |\cos\theta|\right)^2 \quad (1)$$

where r is the particle radius, γ_{ow} is the oil-water interfacial tension, and θ is the contact angle at the three-phase contact line between the two immiscible phases and the absorbed particle. From this expression we can see that the reduction in interfacial energy is strongly a function of particle size and the contact angle at the adsorbed particle's three-phase contact line. However, the contact angle itself does not just control the binding energy of the particle to the interface. Figure 7 depicts a spherical particle bound to the immiscible interface [157]. As described previously, the particle contact angle is dictated by the three-phase contact line and can be solved for pictorially as,

$$\cos(\theta) = \frac{\gamma_{op} - \gamma_{\wp}}{\gamma_{ow}} \quad (2)$$

where γ_{op} and $\gamma_{\wp}$ are the oil-particle and water-particle interfacial tensions. In general, whichever phase contains the largest portion of the particle's volume, this will be the continuous phase for the resulting Pickering emulsion [106,158]. From this, two limits of the particle contact angle arise. For $\theta < 90°$, the particle predominantly resides in the water phase which causes the formation of O/W emulsions. For $\theta > 90°$, the particle predominantly resides in the oil phase which causes the formation of W/O emulsions.

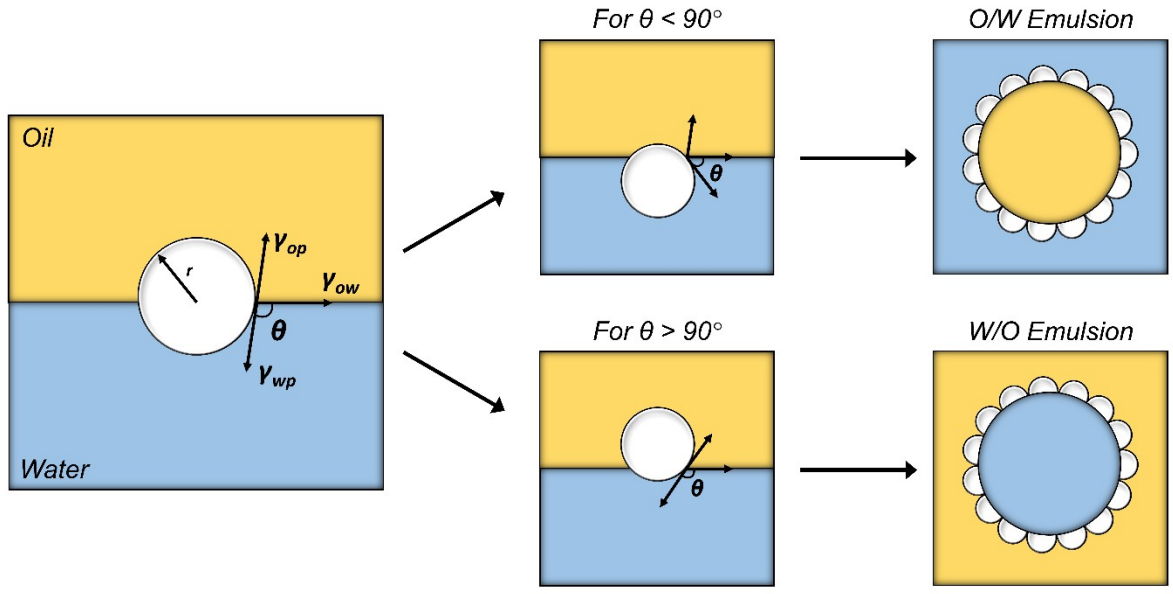

Fig. 7 – A diagram depicting the adsorption of a spherical particle, with radius *r,* to an oil/water interface as a function of the interfacial tensions and the contact angle, θ. For particles where $\theta < 90^\circ$ the resulting emulsion will be an O/W emulsion. For particles where $\theta > 90^\circ$ the resulting emulsion will be a W/O emulsion.

Using these general heuristics, this has led to several developments in the tailored engineering of solid surfactants for Pickering emulsions. One such example is the use of nanoparticle surfactants to form jammed assemblies at oil/water interfaces that can be used for 3D printed all-liquid constructs [159–162]. This strategy was originally developed to strongly bind small nanoparticles to oil/water interfaces because their binding energy is orders of magnitude lower than that of larger particles. In this strategy an electrostatically complimentary ligand is dispersed in the opposite phase of the particles. Electrostatic attractions between the particles and the ligands at the immiscible interface promotes the formation a cooperative assembly. These interactions significantly increase the binding energy of the particles and lowers the systems interfacial tension. However, the dispersal of ligands in the opposite phase is not always ideal. Another strategy is the previously mentioned idea of using amphiphilic Janus particles as solid surfactants. Amphiphilic Janus particles strongly adsorb to oil/water interfaces and can reduce a system's interfacial tension three times more compared to their chemically homogenous counterparts [163]. In addition, one has all the advantages of a solid surfactant while incorporating the amphiphilicity of a small molecule amphiphile. Works that study amphiphilic Janus particles generally focus on probing the equilibrium interfacial configuration and the mechanism of particle assembly at various interfaces. This has resulted in the publication of several articles that cover both these subjects [164–169]. In this section we will discuss using a pendant drop tensiometer to probe the structure of interfacial assemblies and the mechanisms by which they assemble. There are several other techniques one could also use to probe the interfacial behavior of particles, many of which are covered in-depth in other review articles [170–173]. The reader is directed to these to learn more techniques.

A pendant drop tensiometer works by producing a drop of a known size in an immiscible fluid phase hanging from the end of a needle or capillary (Figure 8a) [174–177]. A video of the droplet is then recorded to capture the droplet shape as a function of time. The change in interfacial tension can then be quantified by calculating changes in the droplet radius of

curvature. This can be done using a variety of models, but typically one uses the Young-Laplace method [178]. While this technique appears simple, there are several experimental considerations that must be considered when performing pendant drop experiments. The first is the relative density of the droplet phase to that of the bulk fluid phase. In general, the denser of the two fluids should be contained within the droplet phase while the less dense fluid is the surrounding medium. This allows for the easy formation of a stable drop shape at the end of the capillary or needle. If the densities are reversed, a "J-shaped" needle is used where the less dense droplet is held like a balloon on the end of the needle tip (Figure 8b) [179–181]. Another important experimental parameter is the droplet size. A common way to determine if the droplet size is appropriate for pendant drop measurements is through the calculation of the Bond number. The Bond number is a dimensionless number that describes the importance of gravitational forces relative to interfacial forces and is defined as,

$$B_o = \frac{\Delta \rho g R_c^2}{\gamma} \quad (2)$$

where $\Delta \rho$ is the density difference between the two immiscible fluids, g is acceleration due to gravity, R_c is the radius of curvature of the droplet, and γ is the interfacial tension of the system. Most pendant drop tensiometer computer algorithms calculate interfacial tension on the assumption that the droplet shape is perturbed slightly from spherical. It is then important to ensure that the system is in an appropriate regime of the Bond number such that the assumptions utilized by the fitting algorithms are valid for calculating interfacial tension. [178,182]. However, if the droplet shape becomes too large a stable droplet will not form on the end of the needle and will simply fall off due to gravitational forces. For experiments that occur over extended periods it is important that the droplet size does not change significantly due to evaporation. Evaporation will cause a reduction in the interfacial tension due to a corresponding increase in the areal density of the material adsorbed to the interface with decreasing droplet size. Lastly, systems with ultra-low interfacial tension can be difficult to measure using this method. This is because droplets formed by these systems often just fall off the needle. To get around this limitation one can use very small droplets. However, it is often more appropriate in these situations to use an alternate characterization method such as spinning drop tensiometry [183–185].

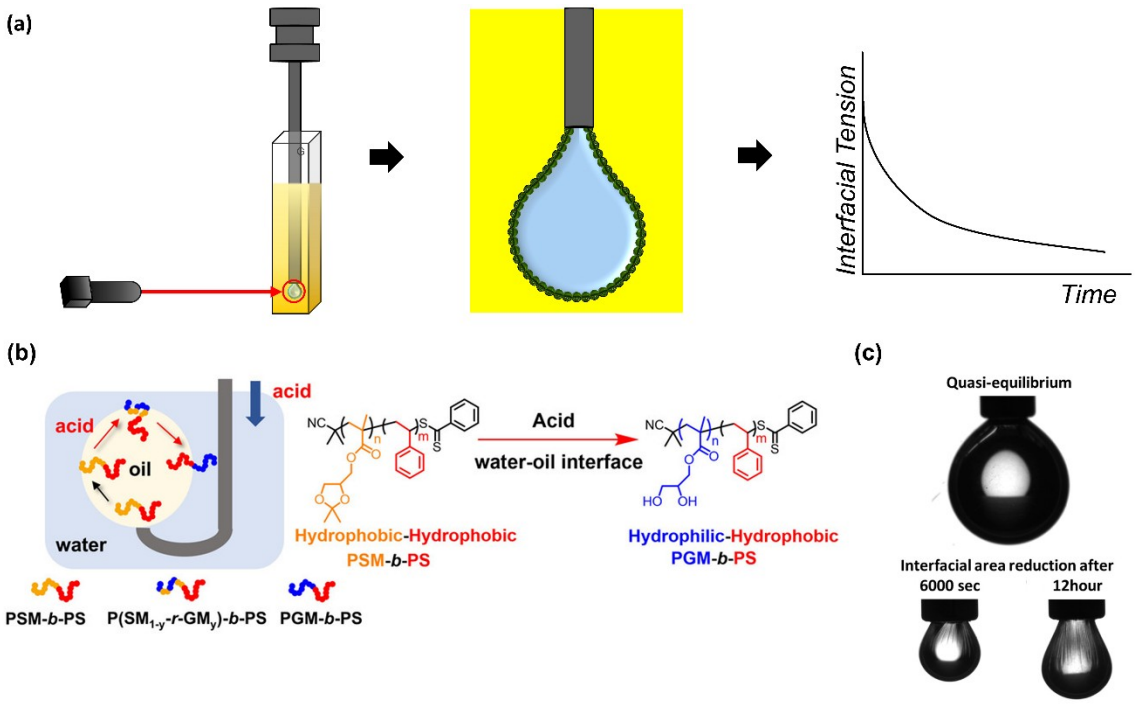

Fig. 8 – (a) A schematic illustrating the pendant drop tensiometer technique and (b) an example system where one can use a "J-shaped" needle in pendant drop experiments. Reproduced with permission [179]. Copyright 2023, Wiley-VCH. Subsequent jamming in these experiments can be observed (c) via the wrinkling of the interface upon the retraction of the droplet and the reduction in interfacial area. Reproduced with permission [186]. Copyright 2017, The American Chemical Society.

Once one has decided on a set of system parameters, there are three common experiments that one can perform using a pendant drop tensiometer. The first experiment is to probe the interfacial tension as a function of time until an equilibrium interfacial tension is attained [187–191]. This allows the simultaneous determination of the equilibrium interfacial tension, but also the kinetics and mechanism of the assembly of materials at the interface. The dynamic interfacial tension curves can then be fit with a series of exponential decay functions (Figure 9a) [179,192,193]. From these fits one can determine the relaxation times for particle adsorption to the interface and any observable phenomena such as particle reconfiguration at the interface. This approach has been used to study the complex adsorption and rearrangement of a wide class of heterogeneous particles and other nanomaterials at fluid interfaces. The second experiment one can perform is pulsating drop interfacial rheology [194–198]. In this experiment, the droplet

volume is sinusoidally increased and decreased while the interfacial tension is recorded. The interfacial tension can then be plotted as a function of frequency and converted to the complex moduli of the interfacial assembly. These complex moduli can then be analyzed to obtain the various relaxation modes of the interfacial assembly for a wide range of surfactant materials. Lastly, one can also perform droplet wrinkling experiments using a pendant drop tensiometer to observe if jamming or other self-wrinkling events occur at the fluid interface [186,192,193,199,200]. This is done by purposefully retracting the droplet from the syringe at a chosen time point in the experiment. If the droplet simply retracts back into the syringe with no change in the droplet morphology, then the assembly is liquid-like and not jammed. If wrinkling of the droplet occurs upon retraction of the droplet, then the assembly at the interface is a jammed assembly. The wavelength of the observed wrinkles can then be used to back calculate the bending modulus and other properties of these jammed assemblies at the droplet interface (Figure 9b) [193,201,202].

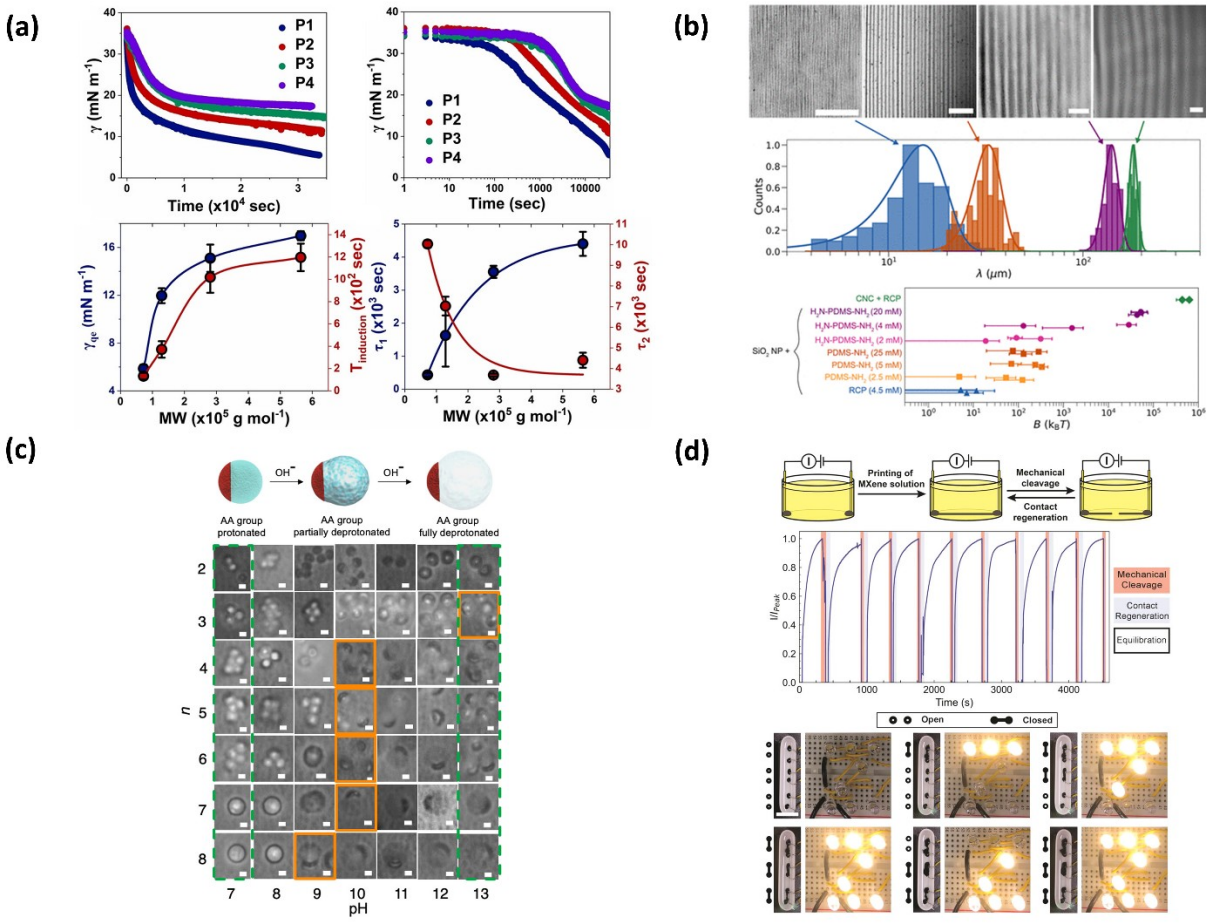

Fig. 9 – Example Pendant Drop analyses where one can perform (a) exponential fitting of dynamic pendant drop tensiometry experiments and (b) wavelength wrinkle analysis to obtain the mechanical properties of fluid interfaces. Reproduced with permission [192,201]. Copyright 2022, Wiley-VCH. Copyright 2021, The American Chemical Society. Example applications of heterogeneous particles at interfaces for used in (a) pH switching Pickering emulsions and (d) all liquid electronics. Reproduced with permission [164,203]. Copyright 2019, The American Chemical Society. Copyright 2023, Wiley-VCH.

Since the development of amphiphilic Janus particles and other heterogeneous particles, a large body of work has been devoted to evaluating their effectiveness as solid surfactants. Several authors have highlighted how the incorporation of Janus characteristics and particle heterogeneity significantly increases the reduction in interfacial energy with particle adsorption to the interface [163,165,167–169]. The total reduction in interfacial energy as well as the resulting properties of Pickering emulsions can easily be tailored by tuning the properties of the particles themselves. One such example is the use of seeded emulsion polymerization to produce amphiphilic Janus particles that are highly amphiphilic and pH responsive [46]. These particles were then used to form highly stable Pickering emulsions which could then flip the emulsion type via a change in the system's pH. Building off this same work, the authors tuned the conditions of seeded emulsion polymerization to cause shifts in the position of the Janus boundary of the particles (Figure 9c) [164]. The change in the position of the Janus boundary also caused changes in the resulting emulsion types one could obtain. In addition, tuning the Janus boundary position also changed when the pH switching behavior occurred within these systems. Another application where heterogeneous particles have been used is the fabrication of 3D printed structured liquids [157,160,204,205]. Through the 3D printing of jammed liquid structures, one can achieve the structural stability of a solid component while retaining all the advantageous transport properties of a liquid medium. These can be used for applications from flow-through chemical reactors [206–212] to 3D printed liquid electronics. One such example is the liquid-in-liquid 3D printing of a jammed MXene structure to form conductive liquid wires (Figure 9d) [203]. These structures were shown to have enough conductivity and stability to function in an electrical circuit and retain their structure over long periods of time. These are just

a few of many examples of the assembly of the various classes of heterogeneous particles at fluid interfaces.

Janus Micromotors

Janus micromotors and nanomotors are Janus particles that exhibit out-of-equilibrium active motion outside of Brownian thermal diffusion. This active motion arises from the interaction of the Janus micromotor with either a self-generated field or an externally imposed field [213–216]. These interactions then lead to the generation anisotropic field gradients around the Janus micromotor which in turn produces propelled motion. The interaction of a particle with an asymmetric field to produce propelled motion can be broadly referred to as phoretic motion. For Janus micromotors that exhibit phoretic motion through a self-generated field, this is often achieved by the chemical decomposition of a fuel. This allows us to then classify Janus micromotors broadly into two separate categories. These are fuel driven systems and field driven systems [217]. By taking advantage of various phoretic mechanisms, a wide range of both fuel-driven and field-driven systems have been produced [218–227].

One of the first reports of autonomous motion from a micromotor-like technology occurred in the early 2000s [228]. In this work, the authors produced self-propelled plates from PDMS slabs where one side was hydrophobic and the other is hydrophilic. A Pt coated porous glass plate was then attached to the hydrophilic side using a steel pin. The plates were then floated on top of an aqueous solution of hydrogen peroxide where the decomposition of the peroxide occurred at the glass plate. This decomposition reaction then generated gaseous bubbles whose release from the glass plate caused the generation of autonomous motion. While this is one of the earliest examples of synthetic autonomous motion, the fabricated plates were comparatively large compared to modern micromotor systems. In addition, these swimmers were not in the form of a Janus particle making it inappropriate to classify it as a Janus micromotor. Several years later, other groups produced the first Janus micromotors in the form of bimetallic Janus rods [229–231]. These rods were shown to self-propel with a persistent ballistic velocity via catalytic electrophoresis. Electrophoresis is phoretic motion that is induced by asymmetric electric field gradients or gradients in charged species around the Janus micromotor.

Several years later authors reported the first example of spherical Janus particles who self-propelled by a combination of catalytic electrophoresis and diffusiophoresis [232]. Diffusiophoresis is phoretic motion that is induced by asymmetric concentration gradients around the surface of the Janus micromotor. The authors also developed one of the first quantitative descriptions of the enhanced random walk behavior commonly observed in single particle tracking of Janus micromotors. Fit functions for calculated mean-squared displacements were developed in which two notable limits could be observed. At times shorter than the characteristic time for Brownian reorientation, the motion of the micromotor was found to exhibit ballistic motion. This implies that the motors were moving with a constant ballistic velocity in a persistent direction up to this characteristic time. At times longer than the characteristic time for Brownian reorientation, the motion of the micromotor was found to be diffusive. This implies that at this characteristic time the motors would change their direction randomly due to the influence of Brownian rotation. This popularized the idea that micromotor motion could be described as an enhanced random walk where each random walk is an individual ballistic propulsion [233–236]. This work established single particle tracking as the gold standard for the characterization of Janus micromotor active motion. However, this technique is limited to the characterization of two-dimensional active motion and limits the size-scale of the particles that can be characterized.

Recently, methods have been developed where dynamic light scattering can be used to characterize the three-dimensional time-dependent active motion of Janus micromotors [67]. It was found that micromotors exhibited enhanced random walk diffusion behavior like that found in single-particle tracking. It was shown that the active motion in these systems was non-steady state and could deplete at a rate that was dependent on the Janus micromotor concentration in the system. Upon complete depletion of fuel, these systems could be refueled to show that fuel driven active motion is also reversible. In both cases, the Janus micromotors in these experiments would exhibit this enhanced random walk diffusion behavior. However, if one desires to suppress this diffusive behavior and achieve directed propulsion, several strategies have been developed to suppress Brownian reorientation [237–243]

Since these early developments, numerous groups have also been actively developing and studying phenomena exhibited by Janus micromotors and other active systems. This has

culminated in the publication of several review articles that cover both developments in the synthesis and characterization of the phenomena associated with non-equilibrium active motion [217,221,223,224,244–251]. In this section we will discuss the common classes of fuel driven and field driven Janus micromotor systems. We will then highlight a unique phenomenon that arises due to this non-equilibrium active motion. Finally, we will discuss some of the applications for which Janus micromotors have been used to showcase their utility and functionality.

A diagram depicting various common classes of fuel- and field-driven micromotor systems can be seen in Figure 10. For fuel-driven micromotor systems, there are several choices of motor and fuel combinations from which one can choose. To achieve fuel driven active motion there are two general requirements one must achieve. First, micromotors are produced containing a Janus or mostly Janus morphology in which one domain is a catalyst for the chosen chemical reaction. Second, the reaction chosen is either a chemical decomposition reaction that produces more products than reactants, or a reaction that produces gaseous products that can form bubbles. The chemical decomposition reaction will produce active motion using either one or a combination of phoretic mechanisms. A reaction that produces large amounts of gaseous bubbles will power the micromotor system using a mechanism known as bubble propulsion [252–257]. In bubble propulsion the release of the bubbles from the surface of the particles produces a strong propulsive force that propels the particles with ballistic motion. As mentioned previously, one of the more popular systems for fuel driven micromotors utilizes a Pt catalyst that chemically decomposes hydrogen peroxide to produce active motion. Since this development other catalyst and fuel combinations have been proposed and utilized such as Ir/hydrazine systems or enzyme powered micromotor systems [112,113,258–265]. These motors typically operate on a phoretic mechanism, but if the motor is large and the reaction product is a gaseous product, these motors can also be powered via bubble propulsion. However, there are micromotor systems that purely operate on a bubble propulsive mechanism. One example is the use of motors where an Mg cube is imbedded in the micromotor as the propulsive component [266–270]. In an aqueous solution, the Mg reacts with the water and produces hydrogen gas that powers the motor via a bubble propulsive mechanism. However, this ultimately causes the

disintegration of the Mg cube imbedded in the motor, limiting the lifetime of operation for these systems.

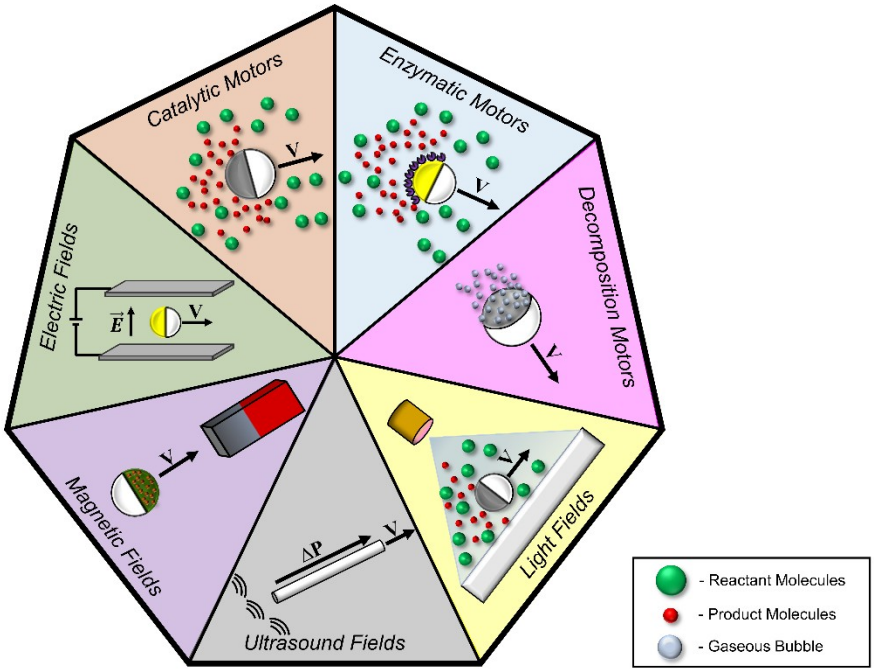

Fig. 10 – A schematic diagram depicting some of the common classes of fuel and field driven micromotor systems.

There are several distinct advantages in using fuel-powered systems. The main advantage is that Janus micromotor motion can be achieved without the use of strong electric, magnetic, light, or ultrasound fields to achieve motion. The requirement of the use of fields has often limited the use of field-driven systems in industrial applications. Fuel driven systems can also be engineered to exhibit diffusive or ballistic motion by choosing the right catalyst/fuel system or by manipulating the geometry of the motor itself. Finally, these motors can often be refueled to produce active motion repeatedly upon the addition of more fuel to the system with little change in the degree of activity. However, there are also several disadvantages to these systems. The requirement of fuel, while an advantage, can also be a disadvantage. The fuels often used for active motion (e.g., hydrogen peroxide or hydrazine) are highly toxic. This limits their use for drug delivery or biological applications. This can be circumvented by using enzyme powered systems where the enzyme's substrate is a non-toxic fuel. However, the stability of the enzymes

over long periods is quite poor and makes enzymatic motors difficult to store for long periods. In addition, micromotors typically designed for various applications usually need to be small. The small size makes Brownian forces large, and the subsequent motion of the micromotors diffusive. The achievement of directed and targeted delivery for small sized motors can be rather difficult without a strong propulsive force, like in the case of bubble propulsion mechanisms. A disadvantage which is specific to motors that operate on this bubble propulsive mechanism is that they are often powered by disintegrating motors that have limited operation lifetimes.

When fabricating field-driven micromotor systems there are several strategies to induce active motion. The most common fields utilized are electric, magnetic, light, or ultrasound fields. There have been a few examples where authors have used thermal fields and thermophoresis to achieve active motion [271–273]. This mechanism is not commonly used due to the requirement of high-powered and high temperature lasers that limit their use and make experimentation difficult. The first example of electrophoretic motors that were powered by an AC electric field were polystyrene/Au Janus micromotors [218,274]. These motors propel themselves perpendicular to the direction of the electric field with a persistent ballistic velocity. These motors are not susceptible to Brownian reorientation due to the large propulsion force generated by the electric field. In a similar manner, magnetic field driven micromotors are ones in which the particle is incorporated with a component that is susceptible to a magnetic field [237,263,275–279]. This is commonly done by incorporating iron-oxide nanoparticles in the particle, or by replacing the catalytic cap in the fuel driven Janus micromotor design with a magnetic one. The motor is then pulled towards the source of the magnetic field with a velocity that increases as the motor swims closer to the magnetic field source. This behavior where the micromotor swims towards the source of the field is known as magnetotaxis [280,281]. Magnetotaxis is often utilized to direct the motion of fuel powered systems by biasing the direction towards the direction of the field. There are other forms of taxis exhibited by micromotor systems, such as chemotaxis [282,283]. These and other forms of taxis exhibited by micromotor systems are discussed extensively in other review articles [224,250,284–287]. Light driven micromotors are ones in which active motion is triggered by the illumination of the micromotor [288–291]. This is often achieved using a light activated catalyst with the motor dispersed in a fuel solution where the reaction only occurs in the presence of the required

wavelength of light. A common example is a TiO_2/hydrogen peroxide motor system in which TiO_2 decomposes hydrogen peroxide under UV illumination at a specific wavelength [292–294]. This allows one to control the motion and activity of the system by shining UV light to trigger or stop the active motion of these species. In recent literature it has been shown that ultrasound can also be used to induce active motion [295–300]. The pressure produced by the sound waves at one end of an anisotropically shaped micromotor can induce fast propulsion. These micromotors can also easily be guided by manipulating the ultrasound source.

Like fuel-driven systems, field-driven systems also offer their own distinct sets of advantages and disadvantages. The first major advantage of field driven systems is that because it is powered by a field, the system can never run out of fuel. As long as the field generation system remains operational, the micromotors will continue to swim under the influence of the field. Along these same lines, this also allows one to circumvent the use of fuels that are potentially toxic to humans and other animals. This has made field-driven systems popular candidates for potential biomedical applications. Many field-driven systems also exhibit directed ballistic propulsion rather than enhanced diffusion behavior. This allows for the direct targeting of specific sites and targets rather than relying on an enhanced diffusion behavior. However, field-driven systems also require the use of large and potentially expensive equipment to generate these fields. This makes these approaches difficult to scale up for applications unless a field source is already in use. In addition, in some applications the use of specific fields is not always the best choice. For example, in a biomedical application it would not be useful to use light powered systems since the light will not easily penetrate human tissue.

Taking both the advantages and disadvantages of fuel- and field-driven systems there have been several micromotor specific phenomena and applications that have been identified. One of the most unique phenomena that has been observed specifically in fuel-driven systems is activity induced phase separation [214,246,301]. This phenomenon occurs when micromotors exhibiting active motion are present in high concentrations either in bulk solution or at a 2D substrate. These micromotors will initially swim as though they are individual motors where the motion of one motor does not influence the other. This is often referred to as a gas-like phase because the Janus micromotors behave like molecules in a gas. However, as time passes the Janus micromotors will begin to swim towards each other and form assemblies whose size,

shape, and symmetry changes over time (Figure 11a) [302,303]. These assemblies are known as reversible active crystals. This is often referred to as a condensed or liquid-like phase because the Janus micromotors are weakly held together like molecules in a liquid phase. This phenomenon arises due to the fuel concentration gradients that are formed in solution upon the triggering of active motion. These concentration gradients cause a flux of fuel to the catalytic surface of the Janus micromotor which produces a molecular fluid flow. These hydrodynamic flows affect the motion of other surrounding Janus micromotors producing a hydrodynamic pumping effect that draws the Janus micromotors to each other. This hydrodynamic pumping effect is responsible for activity induced phase separation in these reversible active crystals. This was confirmed in the original work that reported reversible active crystallization. This was further built upon by others where it was shown that reversible assemblies could be formed with mixtures of active and passive particles (Figure 11b) [294]. The passive colloids would be pulled towards Janus micromotors due to this hydrodynamic pumping effect and form reversible active crystals with Janus micromotors at their core. The symmetry of the crystals could then be tuned by tuning the size ratio of the Janus micromotors to the passive particles. This work shows that the symmetry and type of assemblies can be controlled simply by tuning the properties of the particles in your system. A further degree of control was shown when it was found that these reversible active crystals could be shown to self-assemble into self-spinning microgears [304]. These gears would spin freely and would stay assembled as long as the system remained active. These rotors would then dissipate when the system becomes non-active. The microgears could also be hierarchically assembled to form self-spinning hierarchical rotors made of multiple microgears highlighting the tunability and novelty of these systems.

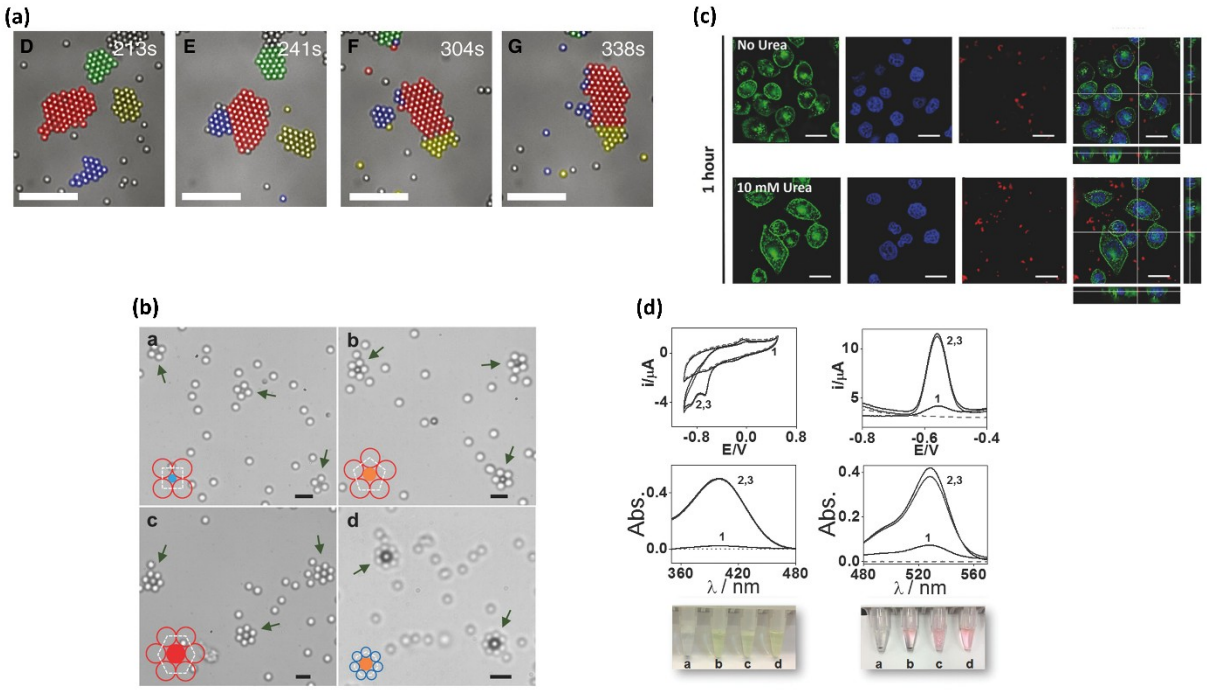

Fig. 11 – Examples of activity induced phase separation where one can see the formation of (a) reversible living crystals containing all Janus micromotors and (b) mixtures of passive and active Janus micromotors. Adapted and reproduced with permission [294,302]. Copyright 2013, The American Association for the Advancement of Science. Copyright 2017, Wiley-VCH. Example applications of Janus micromotors as used in (c) drug delivery applications and as (d) microremediators. Adapted and reproduced with permission [305,306]. Copyright 2017, Wiley-VCH. Copyright 2014, Wiley-VCH.

The main applications for which micromotors have been envisioned are autonomous delivery and clean-up related to drug delivery and environmental remediation applications [307–321]. Several authors have shown the viability for micromotor systems to be used as drug delivery vehicles or as active micro-remediators. One example where micromotors are used as drug delivery vehicles is in Hortelão et al [305]. In this work, mesoporous silica microbots were loaded with doxorubicin and evaluated as drug delivery vehicles (Figure 11c). These microbots are spherical in shape with a size of approximately 344nm. Active motion is achieved through a diffusiophoretic mechanism via the decomposition of urea using urease enzymes attached to the microbot surface. It was found that the urease powered microbots delivered doxorubicin to

HeLA cells more efficiently than their passive counterparts. However, it was still less effective than the use of free doxorubicin. A specific example where Janus micromotors are used as micro-remediators is using activated carbon particles as the non-catalytic portion of a fuel driven Janus micromotor (Figure 11d) [306]. The activated carbon particles were 60 μm spherical particles sputtered with 60 nm of Pt metal. Active motion is achieved through a bubble propulsive mechanism via the generation of oxygen gas bubbles from the decomposition of hydrogen peroxide at the Pt surface. This active motion allowed for the efficient and fast adsorption of a wide range of organic and heavy metal contaminants to the activated carbon Janus micromotors. These are just two specific examples in which Janus micromotors have been used for drug delivery and environmental remediation.

Concluding Remarks and Future Perspective

Within the past few decades there have been several developments towards the synthesis and applications of heterogeneous particles. In this review we have discussed several techniques to fabricate heterogeneous particles and their various applications. Self-assembly and physical vapor deposition is a technique which is amenable to produce Janus or patchy particles in a controllable and consistent manner. However, the technique is limited by its non-scalability and its inability to produce particles of more unique morphologies. Pickering emulsion masking is a method to get around this issue of scalability, but it similarly only produces Janus particles and is often limited to using particles made of silica [105]. Seeded Emulsion polymerization allows one to produce particles of a wide range of morphologies and chemistries while being scalable. However, it requires a large amount of optimization and is limited to producing only polymer particles. Heterogeneous particles that are made using these methods then find extensive use as solid surfactants and as Janus micromotors. We have briefly reviewed how different authors have utilized these systems for responsive emulsions, all liquid electronics, drug delivery vehicles, and environmental remediators.

While there has been extensive research devoted to heterogeneous particle synthesis and their applications, there are several challenges that remain to be addressed. Significant control has been exercised by various groups on producing particles of tailored and controlled morphologies. However, one challenge is producing complex shapes and chemically

heterogeneous particles composed of purely metallic or inorganic components. Most highly shaped heterogeneous particles are usually composed of polymeric or silicate materials. New synthetic techniques need to be continually developed to allow the incorporation of new materials into these particles to potentially expand their application scope [322]. Significant advances have been made in the use of Janus particles and heterogeneous particles as effective solid surfactants. However, these materials are still outperformed by many small molecule surfactants. One notable example is fluorinated surfactants which are extensively used across a broad spectrum of applications ranging from foaming agents to interfacial tension modifiers [323,324]. However, all fluorinated surfactants are or will be completely banned for sale or use in most countries around the world due to their detrimental effects on public health and the environment [325,326]. Continual improvement needs to be made in improving the surfactancy of heterogeneous particles as we continue to look for replacements for these fluorinated materials. The field of Janus micromotors also continues to evolve to yield micromotors with new motors and potential active sources. The major bottleneck preventing Janus micromotors from being used in applications is the lack of techniques to produce them in a scalable manner. This would allow more studies on active motion and collective phenomena that arise due to their active motion.

Conflicts of Interest

The authors have no conflicts of interest to declare.

Acknowledgements

This work was supported the U.S. Department of Energy, Office of Science, Office of Basic Energy Sciences, Materials Sciences and Engineering Division under Contract No. DE-AC02-05-CH11231 within the Adaptive Interfacial Assemblies Towards Structuring Liquids program (KCTR16) and by the National Science Foundation in contract DMR-2104883 and the National Science Foundation under contract 2136955 Structural Control at Fluidic Interfaces with Nano Particle Surfactant Assemblies.

Data Availability

The raw/processed data required to reproduce these results is available upon request from original authors and publishers.

References

[1] W.B. Russel, D.A. Saville, W.R. Schowalter, Colloidal Dispersions, Cambridge University Press, 1989.

[2] P.C. Hiemenz, R. Rajagopalan, Principles of Colloid and Surface Chemistry, Revised and Expanded, CRC Press, 2016.

[3] S.-H. Chen, T.-L. Lin, in: 1987, pp. 489–543.

[4] L. Belloni, Journal of Physics: Condensed Matter 12 (2000) R549–R587.

[5] J. Bibette, F.L. Calderon, P. Poulin, Reports on Progress in Physics 62 (1999) 969–1033.

[6] J. Israelachvili, Colloids Surf A Physicochem Eng Asp 91 (1994) 1–8.

[7] C. Hill, J. Eastoe, Adv Colloid Interface Sci 247 (2017) 496–513.

[8] R.K. Prud'homme, Foams Theory: Measurements: Applications, Routledge, 1996.

[9] J.J. Bikerman, Foams, Springer Berlin Heidelberg, Berlin, Heidelberg, 1973.

[10] M.M.R. (Michael M.R. Williams, S.K. Loyalka, Aerosol Science : Theory and Practice : With Special Applications to the Nuclear Industry, Pergamon Press, 1991.

[11] A. Gurav, T. Kodas, T. Pluym, Y. Xiong, Aerosol Science and Technology 19 (1993) 411–452.

[12] P.G. de Gennes, Science (1979) 256 (1992) 495–497.

[13] T.R. Briggs, Journal of Industrial & Engineering Chemistry 13 (1921) 1008–1010.

[14] A. Gelot, W. Friesen, H.A. Hamza, Colloids and Surfaces 12 (1984) 271–303.

[15] M. Adams-Viola, G.D. Botsaris, Yu.M. Glazman, Colloids and Surfaces 3 (1981) 159–171.

[16] S. Levine, B.D. Bowen, S.J. Partridge, Colloids and Surfaces 38 (1989) 325–343.

[17] J. Zhang, B.A. Grzybowski, S. Granick, Langmuir 33 (2017) 6964–6977.

[18] N. Safaie, R.C. Ferrier, J Appl Phys 127 (2020) 170902.

[19] F. Liang, C. Zhang, Z. Yang, Advanced Materials 26 (2014) 6944–6949.

[20] G. Loget, J. Roche, A. Kuhn, Advanced Materials 24 (2012) 5111–5116.

[21] A. Perro, S. Reculusa, S. Ravaine, E. Bourgeat-Lami, E. Duguet, J Mater Chem 15 (2005) 3745–3760.

[22] F. Liang, C. Zhang, Z. Yang, Advanced Materials 26 (2014) 6944–6949.

[23] Y. Liu, J. Wang, Y. Shao, R. Deng, J. Zhu, Z. Yang, Prog Mater Sci 124 (2022) 100888.

[24] L.C. Bradley, W.H. Chen, K.J. Stebe, D. Lee, Curr Opin Colloid Interface Sci 30 (2017) 25–33.

[25] A. Kumar, B.J. Park, F. Tu, D. Lee, Soft Matter 9 (2013) 6604–6617.

[26] C. Marschelke, A. Fery, A. Synytska, Colloid Polym Sci 298 (2020) 841–865.

[27] T. Maric, M. Zafir, M. Nasir, N.F. Rosli, M. Budanovic, R.D. Webster, N. Cho, M. Pumera, 2000112 (2020) 1–13.

[28] Y. Lan, J. Wu, S.H. Han, S. Yadavali, D. Issadore, K.J. Stebe, D. Lee, ACS Sustain Chem Eng 8 (2020) 17680–17686.

[29] A.B. Pawar, I. Kretzschmar, Macromol Rapid Commun 31 (2010) 150–168.

[30] S. Ravaine, E. Duguet, Curr Opin Colloid Interface Sci 30 (2017) 45–53.

[31] Z. Gong, T. Hueckel, G.-R. Yi, S. Sacanna, Nature 550 (2017) 234–238.

[32] A.B. Pawar, I. Kretzschmar, Langmuir 25 (2009) 9057–9063.

[33] A.B. Pawar, I. Kretzschmar, Langmuir 24 (2008) 355–358.

[34] L. Peng, H. Peng, L. Xu, B. Wang, K. Lan, T. Zhao, R. Che, W. Li, D. Zhao, J Am Chem Soc 144 (2022) 15754–15763.

[35] K.J. Lee, J. Yoon, J. Lahann, Curr Opin Colloid Interface Sci 16 (2011) 195–202.

[36] S. Ravaine, E. Duguet, Curr Opin Colloid Interface Sci 30 (2017) 45–53.

[37] F. Kümmel, B. ten Hagen, R. Wittkowski, I. Buttinoni, R. Eichhorn, G. Volpe, H. Löwen, C. Bechinger, Phys Rev Lett 110 (2013) 198302.

[38] L. Rossi, S. Sacanna, W.T.M. Irvine, P.M. Chaikin, D.J. Pine, A.P. Philipse, Soft Matter 7 (2011) 4139–4142.

[39] X. Zheng, M. Liu, M. He, D.J. Pine, M. Weck, Angewandte Chemie 129 (2017) 5599–5603.

[40] S. Sacanna, W.T.M. Irvine, P.M. Chaikin, D.J. Pine, Nature 464 (2010) 575–578.

[41] J.B. Fan, Y. Song, H. Liu, Z. Lu, F. Zhang, H. Liu, J. Meng, L. Gu, S. Wang, L. Jiang, Sci Adv 3 (2017) 1–9.

[42] W.-H. Chen, F. Tu, L.C. Bradley, D. Lee, Chemistry of Materials 29 (2017) 2685–2688.

[43] Q. Liu, M. Zhao, S. Mytnyk, B. Klemm, K. Zhang, Y. Wang, D. Yan, E. Mendes, J.H. van Esch, Angewandte Chemie 131 (2019) 557–561.

[44] G. Russo, M. Lattuada, J Colloid Interface Sci 611 (2022) 377–389.

[45] L.C. Bradley, K.J. Stebe, D. Lee, J Am Chem Soc 138 (2016) 11437–11440.

[46] F. Tu, D. Lee, J Am Chem Soc 136 (2014) 9999–10006.

[47] H.S.C. Hamilton, L.C. Bradley, Polym Chem 11 (2020) 230–235.

[48] J.-G. Park, J.D. Forster, E.R. Dufresne, J Am Chem Soc 132 (2010) 5960–5961.

[49] J. He, M.J. Hourwitz, Y. Liu, M.T. Perez, Z. Nie, Chemical Communications 47 (2011) 12450.

[50] J.-W. Kim, D. Lee, H.C. Shum, D.A. Weitz, Advanced Materials 20 (2008) 3239–3243.

[51] P.M. Johnson, C.M. van Kats, A. van Blaaderen, Langmuir 21 (2005) 11510–11517.

[52] H. Yu, M. Chen, P.M. Rice, S.X. Wang, R.L. White, S. Sun, Nano Lett 5 (2005) 379–382.

[53] Z. Sun, C. Yang, F. Wang, B. Wu, B. Shao, Z. Li, D. Chen, Z. Yang, K. Liu, Angewandte Chemie 132 (2020) 9451–9455.

[54] C. Ye, X. Yan, X. Dai, R. Chen, Q. Li, S. Xu, Q. Jiang, F. Yan, S. Xu, C.-X. Zhao, P. Zhao, D. Chen, J. Ruan, Chemical Engineering Journal 474 (2023) 145766.

[55] A. Perro, S. Reculusa, E. Bourgeat-Lami, E. Duguet, S. Ravaine, Colloids Surf A Physicochem Eng Asp 284–285 (2006) 78–83.

[56] J.-G. Park, J.D. Forster, E.R. Dufresne, Langmuir 25 (2009) 8903–8906.

[57] D.J. Kraft, J. Hilhorst, M.A.P. Heinen, M.J. Hoogenraad, B. Luigjes, W.K. Kegel, J Phys Chem B 115 (2011) 7175–7181.

[58] W. Yan, M. Pan, J. Yuan, G. Liu, L. Cui, G. Zhang, L. Zhu, Polymer (Guildf) 122 (2017) 139–147.

[59] X. Yu, Y. Sun, F. Liang, B. Jiang, Z. Yang, Macromolecules 52 (2019) 96–102.

[60] Y. Sun, F. Liang, X. Qu, Q. Wang, Z. Yang, Macromolecules 48 (2015) 2715–2722.

[61] R. Hayes, A. Ahmed, T. Edge, H. Zhang, J Chromatogr A 1357 (2014) 36–52.

[62] F.M. Galogahi, Y. Zhu, H. An, N.-T. Nguyen, Journal of Science: Advanced Materials and Devices 5 (2020) 417–435.

[63] R. Ghosh Chaudhuri, S. Paria, Chem Rev 112 (2012) 2373–2433.

[64] J.-M. Rabanel, V. Adibnia, S.F. Tehrani, S. Sanche, P. Hildgen, X. Banquy, C. Ramassamy, Nanoscale 11 (2019) 383–406.

[65] T. Baby, Y. Liu, G. Yang, D. Chen, C.-X. Zhao, J Colloid Interface Sci 594 (2021) 474–484.

[66] F. Liang, J. Liu, C. Zhang, X. Qu, J. Li, Z. Yang, Chem. Commun. 47 (2011) 1231–1233.

[67] A. McGlasson, L.C. Bradley, Small 17 (2021).

[68] H. Takei, N. Shimizu, Langmuir 13 (1997) 1865–1868.

[69] S.C. Thickett, G.H. Teo, Polym Chem 10 (2019) 2906–2924.

[70] R. Arshady, Colloid Polym Sci 270 (1992) 717–732.

[71] J. Qiu, B. Charleux, K. Matyjaszewski, Prog Polym Sci 26 (2001) 2083–2134.

[72] C.S. Chern, Prog Polym Sci 31 (2006) 443–486.

[73] W. Stöber, A. Fink, E. Bohn, J Colloid Interface Sci 26 (1968) 62–69.

[74] P.P. Ghimire, M. Jaroniec, J Colloid Interface Sci 584 (2021) 838–865.

[75] S.-H. Wu, C.-Y. Mou, H.-P. Lin, Chem Soc Rev 42 (2013) 3862.

[76] E.D.E.R. Hyde, A. Seyfaee, F. Neville, R. Moreno-Atanasio, Ind Eng Chem Res 55 (2016) 8891–8913.

[77] Á.A. Beltrán-Osuna, J.E. Perilla, J Solgel Sci Technol 77 (2016) 480–496.

[78] B.G. Prevo, O.D. Velev, Langmuir 20 (2004) 2099–2107.

[79] L. Malaquin, T. Kraus, H. Schmid, E. Delamarche, H. Wolf, Langmuir 23 (2007) 11513–11521.

[80] M.H. Kim, S.H. Im, O.O. Park, Adv Funct Mater 15 (2005) 1329–1335.

[81] A. Qdemat, E. Kentzinger, J. Buitenhuis, U. Rücker, M. Ganeva, T. Brückel, RSC Adv 10 (2020) 18339–18347.

[82] M. Anyfantakis, Z. Geng, M. Morel, S. Rudiuk, D. Baigl, Langmuir 31 (2015) 4113–4120.

[83] J. Park, J. Moon, Langmuir 22 (2006) 3506–3513.

[84] R.D. Deegan, O. Bakajin, T.F. Dupont, G. Huber, S.R. Nagel, T.A. Witten, Nature 389 (1997) 827–829.

[85] R. van Dommelen, P. Fanzio, L. Sasso, Adv Colloid Interface Sci 251 (2018) 97–114.

[86] A. Kaliyaraj Selva Kumar, Y. Zhang, D. Li, R.G. Compton, Electrochem Commun 121 (2020) 106867.

[87] A.D. Dinsmore, J.C. Crocker, A.G. Yodh, Curr Opin Colloid Interface Sci 3 (1998) 5–11.

[88] B.G. Prevo, D.M. Kuncicky, O.D. Velev, Colloids Surf A Physicochem Eng Asp 311 (2007) 2–10.

[89] Z. Chai, A. Childress, A.A. Busnaina, ACS Nano 16 (2022) 17641–17686.

[90] J.A. Thornton, Journal of Vacuum Science & Technology A: Vacuum, Surfaces, and Films 4 (1986) 3059–3065.

[91] J.A. Thornton, SAE Transactions 82 (1973) 1787–1805.

[92] W. Kern, K.K. Schuegraf, in: Handbook of Thin Film Deposition Processes and Techniques, Elsevier, 2001, pp. 11–43.

[93] Z. Wang, Z. Zhang, in: Advanced Nano Deposition Methods, Wiley, 2016, pp. 33–58.

[94] S. Shahidi, B. Moazzenchi, M. Ghoranneviss, The European Physical Journal Applied Physics 71 (2015) 31302.

[95] S. Zeng, K.-T. Yong, I. Roy, X.-Q. Dinh, X. Yu, F. Luan, Plasmonics 6 (2011) 491–506.

[96] V. Poonthiyil, T.K. Lindhorst, V.B. Golovko, A.J. Fairbanks, Beilstein Journal of Organic Chemistry 14 (2018) 11–24.

[97] S.P. Pujari, L. Scheres, A.T.M. Marcelis, H. Zuilhof, Angewandte Chemie International Edition 53 (2014) 6322–6356.

[98] F. Ahangaran, A.H. Navarchian, Adv Colloid Interface Sci 286 (2020) 102298.

[99] A. Liberman, N. Mendez, W.C. Trogler, A.C. Kummel, Surf Sci Rep 69 (2014) 132–158.

[100] H. Li, X. Chen, D. Shen, F. Wu, R. Pleixats, J. Pan, Nanoscale 13 (2021) 15998–16016.

[101] L. Hong, S. Jiang, S. Granick, Langmuir 22 (2006) 9495–9499.

[102] B. Liu, C. Zhang, J. Liu, X. Qu, Z. Yang, Chemical Communications (2009) 3871.

[103] B. Liu, W. Wei, X. Qu, Z. Yang, Angewandte Chemie International Edition 47 (2008) 3973–3975.

[104] A. Perro, F. Meunier, V. Schmitt, S. Ravaine, Colloids Surf A Physicochem Eng Asp 332 (2009) 57–62.

[105] R.J. Archer, A.J. Parnell, A.I. Campbell, J.R. Howse, S.J. Ebbens, Advanced Science 5 (2018) 1700528.

[106] B.P. Binks, Curr Opin Colloid Interface Sci 7 (2002) 21–41.

[107] E.H. Lucassen-Reynders, M. VAN DEN Tempel, J Phys Chem 67 (1963) 731–734.

[108] V.B. Menon, D.T. Wasan, Colloids and Surfaces 29 (1988) 7–27.

[109] D.E. Tambe, M.M. Sharma, Adv Colloid Interface Sci 52 (1994) 1–63.

[110] C. Kaewsaneha, P. Tangboriboonrat, D. Polpanich, M. Eissa, A. Elaissari, Colloids Surf A Physicochem Eng Asp 439 (2013) 35–42.

[111] H. Gu, Z. Yang, J. Gao, C.K. Chang, B. Xu, J Am Chem Soc 127 (2005) 34–35.

[112] X. Ma, A. Jannasch, U.R. Albrecht, K. Hahn, A. Miguel-López, E. Schäffer, S. Sánchez, Nano Lett 15 (2015) 7043–7050.

[113] X. Ma, S. Sánchez, Tetrahedron 73 (2017) 4883–4886.

[114] E.B. Mock, H. De Bruyn, B.S. Hawkett, R.G. Gilbert, C.F. Zukoski, Langmuir 22 (2006) 4037–4043.

[115] J.-G. Park, J.D. Forster, E.R. Dufresne, Langmuir 25 (2009) 8903–8906.

[116] J.-G. Park, J.D. Forster, E.R. Dufresne, J Am Chem Soc 132 (2010) 5960–5961.

[117] M. Okubo, H. Minami, J. Zhou, Colloid Polym Sci 282 (2004) 747–752.

[118] J.K. Oh, J Polym Sci A Polym Chem 46 (2008) 6983–7001.

[119] R. Cordero, A. Jawaid, M.-S. Hsiao, Z. Lequeux, R.A. Vaia, C.K. Ober, ACS Macro Lett 7 (2018) 459–463.

[120] W. Smulders, M.J. Monteiro, Macromolecules 37 (2004) 4474–4483.

[121] S.W. Prescott, M.J. Ballard, E. Rizzardo, R.G. Gilbert, Macromolecules 35 (2002) 5417–5425.

[122] R. Wei, Y. Luo, Z. Li, Polymer (Guildf) 51 (2010) 3879–3886.

[123] J. Guzowski, P.M. Korczyk, S. Jakiela, P. Garstecki, Soft Matter 8 (2012) 7269–7278.

[124] A. Walther, A.H.E. Müller, Soft Matter 4 (2008) 663.

[125] A.H. Gröschel, A. Walther, T.I. Löbling, F.H. Schacher, H. Schmalz, A.H.E. Müller, Nature 503 (2013) 247–251.

[126] A. Walther, A.H.E. Müller, Chem Rev 113 (2013) 5194–5261.

[127] Liu, V. Abetz, A.H.E. Müller, Macromolecules 36 (2003) 7894–7898.

[128] A. Walther, X. André, M. Drechsler, V. Abetz, A.H.E. Müller, J Am Chem Soc 129 (2007) 6187–6198.

[129] R. Erhardt, M. Zhang, A. Böker, H. Zettl, C. Abetz, P. Frederik, G. Krausch, V. Abetz, A.H.E. Müller, J Am Chem Soc 125 (2003) 3260–3267.

[130] R. Erhardt, A. Böker, H. Zettl, H. Kaya, W. Pyckhout-Hintzen, G. Krausch, V. Abetz, A.H.E. Müller, Macromolecules 34 (2001) 1069–1075.

[131] R. Deng, F. Liang, X. Qu, Q. Wang, J. Zhu, Z. Yang, Macromolecules 48 (2015) 750–755.

[132] R. Deng, F. Liang, W. Li, S. Liu, R. Liang, M. Cai, Z. Yang, J. Zhu, Small 9 (2013) 4099–4103.

[133] R. Deng, F. Liang, P. Zhou, C. Zhang, X. Qu, Q. Wang, J. Li, J. Zhu, Z. Yang, Advanced Materials 26 (2014) 4469–4472.

[134] R. Deng, F. Liang, W. Li, Z. Yang, J. Zhu, Macromolecules 46 (2013) 7012–7017.

[135] D. Hu, X. Chang, Y. Xu, Q. Yu, Y. Zhu, ACS Macro Lett 10 (2021) 914–920.

[136] J.T. Davies, E.K. Rideal, Interfacial Phenomena, Elsevier, 1961.

[137] E. Hadjittofis, S.C. Das, G.G.Z. Zhang, J.Y.Y. Heng, in: Developing Solid Oral Dosage Forms, Elsevier, 2017, pp. 225–252.

[138] C.A. Miller, P. Neogi, Interfacial Phenomena, CRC Press, 2007.

[139] H.L. Halliday, Journal of Perinatology 28 (2008) S47–S56.

[140] M.R. Porter, Handbook of Surfactants, Springer US, Boston, MA, 1991.

[141] M.J. Rosen, J.T. Kunjappu, Surfactants and Interfacial Phenomena, Wiley, 2012.

[142] T.F. Tadros, Applied Surfactants, Wiley, 2005.

[143] W. Ramsden, Proceedings of the Royal Society of London 72 (1904) 156–164.

[144] S.U. Pickering, J. Chem. Soc., Trans. 91 (1907) 2001–2021.

[145] C.C. Berton-Carabin, K. Schroën, Annu Rev Food Sci Technol 6 (2015) 263–297.

[146] J. Wu, G.H. Ma, Small 12 (2016) 4633–4648.

[147] D. Gonzalez Ortiz, C. Pochat-Bohatier, J. Cambedouzou, M. Bechelany, P. Miele, Engineering 6 (2020) 468–482.

[148] L.E. Low, S.P. Siva, Y.K. Ho, E.S. Chan, B.T. Tey, Adv Colloid Interface Sci 277 (2020).

[149] B.P. Binks, S.O. Lumsdon, Langmuir 17 (2001) 4540–4547.

[150] B.P. Binks, S.O. Lumsdon, Langmuir 16 (2000) 2539–2547.

[151] B.P. Binks, S.O. Lumsdon, Langmuir 16 (2000) 8622–8631.

[152] B.P. Binks, S.O. Lumsdon, Physical Chemistry Chemical Physics 1 (1999) 3007–3016.

[153] L. Chen, Y. Xiao, Q. Wu, X. Yan, P. Zhao, J. Ruan, J. Shan, D. Chen, D.A. Weitz, F. Ye, Small 17 (2021).

[154] H. He, F. Liang, Chemistry of Materials 34 (2022) 3806–3818.

[155] Y. Wu, C. Zhang, X. Qu, Z. Liu, Z. Yang, Langmuir 26 (2010) 9442–9448.

[156] A. Koretsky, P. Kruglyakov, Izv. Sib. Otd. Akad. Nauk USSR 2 (1971) 139.

[157] J. Forth, P.Y. Kim, G. Xie, X. Liu, B.A. Helms, T.P. Russell, Advanced Materials 31 (2019) 1806370.

[158] R. Aveyard, B.P. Binks, J.H. Clint, Emulsions Stabilised Solely by Colloidal Particles, 2003.

[159] M. Cui, T. Emrick, T.P. Russell, Science (1979) 342 (2013) 460–463.

[160] J. Forth, X. Liu, J. Hasnain, A. Toor, K. Miszta, S. Shi, P.L. Geissler, T. Emrick, B.A. Helms, T.P. Russell, Advanced Materials 30 (2018).

[161] C. Huang, Z. Sun, M. Cui, F. Liu, B.A. Helms, T.P. Russell, Advanced Materials 28 (2016) 6612–6618.

[162] Z. Fink, X. Wu, P.Y. Kim, A. McGlasson, M. Abdelsamie, T. Emrick, C.M. Sutter-Fella, P.D. Ashby, B.A. Helms, T.P. Russell, Small (2023).

[163] B.P. Binks, P.D.I. Fletcher, Langmuir 17 (2001) 4708–4710.

[164] Y. Lan, J. Choi, H. Li, Y. Jia, R. Huang, K.J. Stebe, D. Lee, Ind Eng Chem Res 58 (2019) 20961–20968.

[165] B.J. Park, T. Brugarolas, D. Lee, Soft Matter 7 (2011) 6413–6417.

[166] B.J. Park, C.H. Choi, S.M. Kang, K.E. Tettey, C.S. Lee, D. Lee, Langmuir 29 (2013) 1841–1849.

[167] S. Razavi, L.M. Hernandez, A. Read, W.L. Vargas, I. Kretzschmar, J Colloid Interface Sci 558 (2019) 95–99.

[168] S. Razavi, B. Lin, K.Y.C. Lee, R.S. Tu, I. Kretzschmar, Langmuir 35 (2019) 15813–15824.

[169] N. Glaser, D.J. Adams, A. Böker, G. Krausch, Langmuir 22 (2006) 5227–5229.

[170] K. Koynov, H.-J. Butt, Curr Opin Colloid Interface Sci 17 (2012) 377–387.

[171] J. Daillant, Curr Opin Colloid Interface Sci 14 (2009) 396–401.

[172] O.N. Oliveira, L. Caseli, K. Ariga, Chem Rev 122 (2022) 6459–6513.

[173] E.I. Franses, O.A. Basaran, C.-H. Chang, Curr Opin Colloid Interface Sci 1 (1996) 296–303.

[174] E.I. Franses, O.A. Basaran, C.-H. Chang, Curr Opin Colloid Interface Sci 1 (1996) 296–303.

[175] C.E. Stauffer, J Phys Chem 69 (1965) 1933–1938.

[176] G. Faour, M. Grimaldi, J. Richou, A. Bois, J Colloid Interface Sci 181 (1996) 385–392.

[177] J.D. Berry, M.J. Neeson, R.R. Dagastine, D.Y.C. Chan, R.F. Tabor, J Colloid Interface Sci 454 (2015) 226–237.

[178] N.J. Alvarez, L.M. Walker, S.L. Anna, Langmuir 26 (2010) 13310–13319.

[179] Z. Chen, M. Hu, X. Li, D.M. Smith, H. Seong, T. Emrick, J. Rzayev, T.P. Russell, Angewandte Chemie International Edition 61 (2022).

[180] S.-Y. Lin, H.-F. Hwang, Langmuir 10 (1994) 4703–4709.

[181] S.-Y. Lin, T.-L. Lu, W.-B. Hwang, Langmuir 11 (1995) 555–562.

[182] A. Morita, D. Carastan, N. Demarquette, Colloid Polym Sci 280 (2002) 857–864.

[183] H.H. Hu, D.D. Joseph, J Colloid Interface Sci 162 (1994) 331–339.

[184] B. Gash, D.R. Parrish, Journal of Petroleum Technology 29 (1977) 30–31.

[185] J.A. Pojman, C. Whitmore, M.L. Turco Liveri, R. Lombardo, J. Marszalek, R. Parker, B. Zoltowski, Langmuir 22 (2006) 2569–2577.

[186] Y. Jiang, T.I. Löbling, C. Huang, Z. Sun, A.H.E. Müller, T.P. Russell, ACS Appl Mater Interfaces 9 (2017) 33327–33332.

[187] L. Liggieri, F. Ravera, A. Passerone, J Colloid Interface Sci 169 (1995) 238–240.

[188] M. Nobakht, S. Moghadam, Y. Gu, Ind Eng Chem Res 47 (2008) 8918–8925.

[189] Z. Zhao, C. Bi, W. Qiao, Z. Li, L. Cheng, Colloids Surf A Physicochem Eng Asp 294 (2007) 191–202.

[190] H. Li, D. Yang, P. Tontiwachwuthikul, Energy & Fuels 26 (2012) 1776–1786.

[191] R. Miller, E.V. Aksenenko, V.B. Fainerman, Adv Colloid Interface Sci 247 (2017) 115–129.

[192] H.G. Seong, Z. Chen, T. Emrick, T.P. Russell, Angewandte Chemie - International Edition 61 (2022).

[193] H.G. Seong, Z. Fink, Z. Chen, T. Emrick, T.P. Russell, ACS Nano 17 (2023) 14731–14741.

[194] M. A. Bos, T. van Vliet, Adv Colloid Interface Sci 91 (2001) 437–471.

[195] B.S. Murray, Curr Opin Colloid Interface Sci 7 (2002) 426–431.

[196] J. Maldonado-Valderrama, J.M.R. Patino, Curr Opin Colloid Interface Sci 15 (2010) 271–282.

[197] A.J. Mendoza, E. Guzmán, F. Martínez-Pedrero, H. Ritacco, R.G. Rubio, F. Ortega, V.M. Starov, R. Miller, Adv Colloid Interface Sci 206 (2014) 303–319.

[198] J.P. Rane, V. Pauchard, A. Couzis, S. Banerjee, Langmuir 29 (2013) 4750–4759.

[199] Y. Jiang, R. Chakroun, P. Gu, A.H. Gröschel, T.P. Russell, Angewandte Chemie - International Edition 59 (2020) 12751–12755.

[200] Z. Sun, T. Feng, T.P. Russell, Langmuir 29 (2013) 13407–13413.

[201] J. Forth, A. Mariano, Y. Chai, A. Toor, J. Hasnain, Y. Jiang, W. Feng, X. Liu, P.L. Geissler, N. Menon, B.A. Helms, P.D. Ashby, T.P. Russell, Nano Lett 21 (2021) 7116–7122.

[202] D.J. Fesenmeier, S. Park, S. Kim, Y.-Y. Won, J Colloid Interface Sci 617 (2022) 764–777.

[203] D. Popple, M. Shekhirev, C. Dai, P. Kim, K.X. Wang, P. Ashby, B.A. Helms, Y. Gogotsi, T.P. Russell, A. Zettl, Advanced Materials (2022) 2208148.

[204] S. Shi, X. Liu, Y. Li, X. Wu, D. Wang, J. Forth, T.P. Russell, Advanced Materials 30 (2018).

[205] X. Liu, S. Shi, Y. Li, J. Forth, D. Wang, T.P. Russell, Angewandte Chemie 129 (2017) 12768–12772.

[206] R. Zhao, T. Han, D. Sun, L. Huang, F. Liang, Z. Liu, Langmuir 35 (2019) 11435–11442.

[207] R. Zhao, X. Yu, D. Sun, L. Huang, F. Liang, Z. Liu, ACS Appl Nano Mater 2 (2019) 2127–2132.

[208] M. Zhang, R. Ettelaie, T. Yan, S. Zhang, F. Cheng, B.P. Binks, H. Yang, J Am Chem Soc 139 (2017) 17387–17396.

[209] L. Wei, M. Zhang, X. Zhang, H. Xin, H. Yang, ACS Sustain Chem Eng 4 (2016) 6838–6843.

[210] T. Yang, L. Wei, L. Jing, J. Liang, X. Zhang, M. Tang, M.J. Monteiro, Y. (Ian) Chen, Y. Wang, S. Gu, D. Zhao, H. Yang, J. Liu, G.Q.M. Lu, Angewandte Chemie International Edition 56 (2017) 8459–8463.

[211] M. Zhang, L. Wei, H. Chen, Z. Du, B.P. Binks, H. Yang, J Am Chem Soc 138 (2016) 10173–10183.

[212] H. Yang, L. Fu, L. Wei, J. Liang, B.P. Binks, J Am Chem Soc 137 (2015) 1362–1371.

[213] J. Elgeti, R.G. Winkler, G. Gompper, Reports on Progress in Physics 78 (2015).

[214] P. Illien, R. Golestanian, A. Sen, Chem Soc Rev 46 (2017) 5508–5518.

[215] J.L. Moran, J.D. Posner, Annu Rev Fluid Mech 49 (2017) 511–540.

[216] X. Lin, Z. Wu, Y. Wu, M. Xuan, Q. He, Advanced Materials 28 (2016) 1060–1072.

[217] M. Fernández-Medina, M.A. Ramos-Docampo, O. Hovorka, V. Salgueiriño, B. Städler, Adv Funct Mater 30 (2020) 1908283.

[218] N.M. Diwakar, G. Kunti, T. Miloh, G. Yossifon, O.D. Velev, Curr Opin Colloid Interface Sci 59 (2022).

[219] M. Yan, K. Liang, D. Zhao, B. Kong, Small 2102887 (2021) 2102887.

[220] W.F. Paxton, S. Sundararajan, T.E. Mallouk, A. Sen, Angewandte Chemie - International Edition 45 (2006) 5420–5429.

[221] S. Sanchez, L. Soler, J. Katuri, Angewandte Chemie - International Edition 54 (2015) 1414–1444.

[222] S.J. Ebbens, J.R. Howse, Soft Matter 6 (2010) 726–738.

[223] A.M. Pourrahimi, M. Pumera, Nanoscale 10 (2018) 16398–16415.

[224] J. Agudo-Canalejo, T. Adeleke-Larodo, P. Illien, R. Golestanian, Acc Chem Res 51 (2018) 2365–2372.

[225] S.J. Ebbens, D.A. Gregory, Acc Chem Res 51 (2018) 1931–1939.

[226] B. Robertson, M.J. Huang, J.X. Chen, R. Kapral, Acc Chem Res 51 (2018) 2355–2364.

[227] H. Wang, M. Pumera, Chem Rev 115 (2015) 8704–8735.

[228] R.F. Ismagilov, A. Schwartz, N. Bowden, G.M. Whitesides, Angewandte Chemie - International Edition 41 (2002) 652–654.

[229] W.F. Paxton, K.C. Kistler, C.C. Olmeda, A. Sen, S.K. St. Angelo, Y. Cao, T.E. Mallouk, P.E. Lammert, V.H. Crespi, J Am Chem Soc 126 (2004) 13424–13431.

[230] W.F. Paxton, K.C. Kistler, C.C. Olmeda, A. Sen, S.K. St. Angelo, Y. Cao, T.E. Mallouk, P.E. Lammert, V.H. Crespi, J Am Chem Soc 126 (2004) 13424–13431.

[231] W.F. Paxton, P.T. Baker, T.R. Kline, Y. Wang, T.E. Mallouk, A. Sen, J Am Chem Soc 128 (2006) 14881–14888.

[232] J.R. Howse, R.A.L. Jones, A.J. Ryan, T. Gough, R. Vafabakhsh, R. Golestanian, Phys Rev Lett 99 (2007) 8–11.

[233] D.A. Gregory, A.I. Campbell, S.J. Ebbens, Journal of Physical Chemistry C 119 (2015) 15339–15348.

[234] S.J. Ebbens, J.R. Howse, Langmuir 27 (2011) 12293–12296.

[235] T.C. Lee, M. Alarcón-Correa, C. Miksch, K. Hahn, J.G. Gibbs, P. Fischer, Nano Lett 14 (2014) 2407–2412.

[236] C. Kurzthaler, C. Devailly, J. Arlt, T. Franosch, W.C.K. Poon, V.A. Martinez, A.T. Brown, Phys Rev Lett 121 (2018) 1–6.

[237] P.S. Schattling, M.A. Ramos-Docampo, V. Salgueiriño, B. Städler, ACS Nano 11 (2017) 3973–3983.

[238] S. Das, A. Garg, A.I. Campbell, J. Howse, A. Sen, D. Velegol, R. Golestanian, S.J. Ebbens, Nat Commun 6 (2015) 1–10.

[239] X. Ma, S. Jang, M.N. Popescu, W.E. Uspal, A. Miguel-López, K. Hahn, D.P. Kim, S. Sánchez, ACS Nano 10 (2016) 8751–8759.

[240] A. Mozaffari, N. Sharifi-Mood, J. Koplik, C. Maldarelli, Physics of Fluids 28 (2016) 053107.

[241] K. Dietrich, D. Renggli, M. Zanini, G. Volpe, I. Buttinoni, L. Isa, New J Phys 19 (2017) 065008.

[242] Z. Jalilvand, H. Haider, J. Cui, and I. Kretzschmar, Langmuir 36 (2020) 6880–6887.

[243] A.D. Fusi, Y. Li, A. Llopis-Lorente, T. Patiño, J.C.M. van Hest, L.K.E.A. Abdelmohsen, Angewandte Chemie - International Edition 62 (2023).

[244] F. Novotný, M. Pumera, Sci Rep 9 (2019) 13222.

[245] W. Wang, T.E. Mallouk, ACS Nano 15 (2021) 15446–15460.

[246] W. Wang, W. Duan, S. Ahmed, A. Sen, T.E. Mallouk, Acc Chem Res 48 (2015) 1938–1946.

[247] N.L. Abbott, O.D. Velev, Curr Opin Colloid Interface Sci 21 (2016) 1–3.

[248] W. Fei, Y. Gu, K.J.M. Bishop, Curr Opin Colloid Interface Sci 32 (2017) 57–68.

[249] B. Esteban-Fernández De Ávila, W. Gao, E. Karshalev, L. Zhang, J. Wang, Acc Chem Res 51 (2018) 1901–1910.

[250] M. You, C. Chen, L. Xu, F. Mou, J. Guan, Acc Chem Res 51 (2018) 3006–3014.

[251] A.M. Pourrahimi, M. Pumera, Nanoscale 10 (2018) 16398–16415.

[252] J.G. Gibbs, Y.-P. Zhao, Appl Phys Lett 94 (2009).

[253] H. Wang, J.G.S. Moo, M. Pumera, ACS Nano 10 (2016) 5041–5050.

[254] J. Li, X. Zhai, Z. Yang, Z. Pei, M. Luo, J. Guan, J Mater Chem C Mater 11 (2023) 7059–7067.

[255] S. Wang, N. Wu, Langmuir 30 (2014) 3477–3486.

[256] Z. Wu, Y. Wu, W. He, X. Lin, J. Sun, Q. He, Angewandte Chemie International Edition 52 (2013) 7000–7003.

[257] Y. Wu, Z. Wu, X. Lin, Q. He, J. Li, ACS Nano 6 (2012) 10910–10916.

[258] R. Dong, J. Li, I. Rozen, B. Ezhilan, T. Xu, C. Christianson, W. Gao, D. Saintillan, B. Ren, J. Wang, Sci Rep 5 (2015) 1–7.

[259] W. Gao, A. Pei, R. Dong, J. Wang, J Am Chem Soc 136 (2014) 2276–2279.

[260] M.E. Ibele, Y. Wang, T.R. Kline, T.E. Mallouk, A. Sen, J Am Chem Soc 129 (2007) 7762–7763.

[261] T. Patino, X. Arqué, R. Mestre, L. Palacios, S. Sánchez, Acc Chem Res 51 (2018) 2662–2671.

[262] X. Zhao, K. Gentile, F. Mohajerani, A. Sen, Acc Chem Res 51 (2018) 2373–2381.

[263] M. Luo, S. Li, J. Wan, C. Yang, B. Chen, J. Guan, Langmuir 36 (2020) acs.langmuir.9b03315.

[264] T. Patiño, N. Feiner-Gracia, X. Arqué, A. Miguel-López, A. Jannasch, T. Stumpp, E. Schäffer, L. Albertazzi, S. Sánchez, J Am Chem Soc 140 (2018) 7896–7903.

[265] Z. Yang, L. Wang, Z. Gao, X. Hao, M. Luo, Z. Yu, J. Guan, ACS Nano (2023).

[266] C. Chen, E. Karshalev, J. Guan, J. Wang, Small 14 (2018) 1–10.

[267] Z. Zhao, T. Si, A.I. Kozelskaya, I.O. Akimchenko, S.I. Tverdokhlebov, S. Rutkowski, J. Frueh, Colloids Surf B Biointerfaces 218 (2022).

[268] C. Chen, E. Karshalev, J. Guan, J. Wang, Small 14 (2018).

[269] W. Gao, X. Feng, A. Pei, Y. Gu, J. Li, J. Wang, Nanoscale 5 (2013) 4696.

[270] F. Mou, C. Chen, H. Ma, Y. Yin, Q. Wu, J. Guan, Angewandte Chemie International Edition 52 (2013) 7208–7212.

[271] D. Rings, R. Schachoff, M. Selmke, F. Cichos, K. Kroy, Phys Rev Lett 105 (2010) 090604.

[272] A.P. Bregulla, F. Cichos, J Chem Phys 151 (2019).

[273] K. Kroy, D. Chakraborty, F. Cichos, Eur Phys J Spec Top 225 (2016) 2207–2225.

[274] S. Gangwal, O.J. Cayre, M.Z. Bazant, O.D. Velev, Phys Rev Lett 100 (2008).

[275] W. Gao, D. Kagan, O.S. Pak, C. Clawson, S. Campuzano, E. Chuluun-Erdene, E. Shipton, E.E. Fullerton, L. Zhang, E. Lauga, J. Wang, Small 8 (2012) 460–467.

[276] G. Kokot, A. Sokolov, A. Snezhko, Langmuir 36 (2020) 6957–6962.

[277] S. Büttgenbach, Micromachines (Basel) 5 (2014) 929–942.

[278] H. Xu, M. Medina-Sánchez, O.G. Schmidt, Angewandte Chemie International Edition 59 (2020) 15029–15037.

[279] H. Xie, M. Sun, X. Fan, Z. Lin, W. Chen, L. Wang, L. Dong, Q. He, Sci Robot 4 (2019).

[280] H.G.P.L. de Barros, D.M.S. Esquivel, M. Farina, Science Progress (1933-) 74 (1990) 347–359.

[281] B. Wang, Y. Qin, J. Liu, Z. Zhang, W. Li, G. Pu, Z. Yuanhe, X. Gui, M. Chu, ACS Appl Mater Interfaces 15 (2023) 2747–2759.

[282] J. Shao, M. Xuan, H. Zhang, X. Lin, Z. Wu, Q. He, Angewandte Chemie 129 (2017) 13115–13119.

[283] C. Chen, X. Chang, P. Angsantikul, J. Li, B. Esteban-Fernández de Ávila, E. Karshalev, W. Liu, F. Mou, S. He, R. Castillo, Y. Liang, J. Guan, L. Zhang, J. Wang, Adv Biosyst 2 (2018).

[284] G. Zhao, S. Sanchez, O.G. Schmidt, M. Pumera, Chemical Communications 48 (2012) 10090.

[285] L. Huang, J.L. Moran, W. Wang, JCIS Open 2 (2021) 100006.

[286] K. Yuan, M. Pacheco, B. Jurado-Sánchez, A. Escarpa, Advanced Intelligent Systems 3 (2021).

[287] C. Gao, Y. Feng, D.A. Wilson, Y. Tu, F. Peng, Small 18 (2022).

[288] J. Wang, Z. Xiong, J. Zheng, X. Zhan, J. Tang, Acc Chem Res 51 (2018) 1957–1965.

[289] J. Wang, Z. Xiong, J. Tang, Advanced Intelligent Systems 2000170 (2021) 2000170.

[290] L. Kong, C.C. Mayorga-Martinez, J. Guan, M. Pumera, Small 16 (2020) 1–14.

[291] M. Xuan, Z. Wu, J. Shao, L. Dai, T. Si, Q. He, J Am Chem Soc 138 (2016) 6492–6497.

[292] U. Choudhury, D.P. Singh, T. Qiu, P. Fischer, Advanced Materials 31 (2019) 1–7.

[293] L. Kong, C.C. Mayorga-Martinez, J. Guan, M. Pumera, ACS Appl Mater Interfaces 10 (2018) 22427–22434.

[294] D.P. Singh, U. Choudhury, P. Fischer, A.G. Mark, Advanced Materials 29 (2017) 1701328.

[295] L. Ren, W. Wang, T.E. Mallouk, Acc Chem Res 51 (2018) 1948–1956.

[296] L.M. Johnson, L. Gao, C.W. Shields IV, M. Smith, K. Efimenko, K. Cushing, J. Genzer, G.P. López, J Nanobiotechnology 11 (2013) 22.

[297] M. Valdez-Garduño, M. Leal-Estrada, E.S. Oliveros-Mata, D.I. Sandoval-Bojorquez, F. Soto, J. Wang, V. Garcia-Gradilla, Adv Funct Mater 30 (2020).

[298] W. Cao, Y. Liu, P. Ran, J. He, S. Xie, J. Weng, X. Li, ACS Appl Mater Interfaces 13 (2021) 58411–58421.

[299] A. Aziz, J. Holthof, S. Meyer, O.G. Schmidt, M. Medina-Sánchez, Adv Healthc Mater 10 (2021).

[300] W. Wang, W. Duan, Z. Zhang, M. Sun, A. Sen, T.E. Mallouk, Chemical Communications 51 (2015) 1020–1023.

[301] M.N. Popescu, Langmuir 36 (2020) 6861–6870.

[302] J. Palacci, S. Sacanna, A.P. Steinberg, D.J. Pine, P.M. Chaikin, Science (1979) 339 (2013) 936–940.

[303] J. Palacci, S. Sacanna, S.-H. Kim, G.-R. Yi, D.J. Pine, P.M. Chaikin, Philosophical Transactions of the Royal Society A: Mathematical, Physical and Engineering Sciences 372 (2014) 20130372.

[304] A. Aubret, M. Youssef, S. Sacanna, J. Palacci, Nat Phys 14 (2018) 1114–1118.

[305] A.C. Hortelão, T. Patiño, A. Perez-Jiménez, À. Blanco, S. Sánchez, Adv Funct Mater 28 (2018) 1705086.

[306] B. Jurado-Sánchez, S. Sattayasamitsathit, W. Gao, L. Santos, Y. Fedorak, V. V. Singh, J. Orozco, M. Galarnyk, J. Wang, Small 11 (2015) 499–506.

[307] M. Zarei, M. Zarei, Small 14 (2018) 1–17.

[308] D. Xu, Y. Wang, C. Liang, Y. You, S. Sanchez, X. Ma, Small 16 (2020) 1–22.

[309] A. Somasundar, A. Sen, Small 17 (2021) 1–7.

[310] J. Wang, Z. Xiong, J. Zheng, X. Zhan, J. Tang, Acc Chem Res 51 (2018) 1957–1965.

[311] L. Wang, S. Song, J. van Hest, L.K.E.A. Abdelmohsen, X. Huang, S. Sánchez, Small 1907680 (2020) 1–19.

[312] C.P. Thome, W.S. Hoertdoerfer, J.R. Bendorf, J.G. Lee, C.W. Shields, Nano Lett (2023).

[313] J.G. Lee, R.R. Raj, N.B. Day, C.W. Shields, ACS Nano (2023).

[314] Y. Hu, W. Liu, Y. Sun, Adv Funct Mater 32 (2022).

[315] D. Vilela, M.M. Stanton, J. Parmar, S. Sánchez, ACS Appl Mater Interfaces 9 (2017) 22093–22100.

[316] B.E.F. De Ávila, P. Angsantikul, J. Li, M. Angel Lopez-Ramirez, D.E. Ramírez-Herrera, S. Thamphiwatana, C. Chen, J. Delezuk, R. Samakapiruk, V. Ramez, L. Zhang, J. Wang, Nat Commun 8 (2017).

[317] G. Xie, P. Li, P.Y. Kim, P.-Y. Gu, B.A. Helms, P.D. Ashby, L. Jiang, T.P. Russell, Nat Chem (2021).

[318] S. Sattayasamitsathit, H. Kou, W. Gao, W. Thavarajah, K. Kaufmann, L. Zhang, J. Wang, Small 10 (2014) 2830–2833.

[319] F. Striggow, M. Medina-Sánchez, G.K. Auernhammer, V. Magdanz, B.M. Friedrich, O.G. Schmidt, Small 16 (2020).

[320] B. Esteban-Fernández de Ávila, P. Angsantikul, J. Li, W. Gao, L. Zhang, J. Wang, Adv Funct Mater 28 (2018) 1–12.

[321] M. Luo, Y. Feng, T. Wang, J. Guan, Adv Funct Mater 28 (2018) 1–23.

[322] Y. Yu, R. Lin, H. Yu, M. Liu, E. Xing, W. Wang, F. Zhang, D. Zhao, X. Li, Nat Commun 14 (2023) 4249.

[323] S.M.S. Hussain, A.A. Adewunmi, A. Mahboob, M. Murtaza, X. Zhou, M.S. Kamal, Adv Colloid Interface Sci 303 (2022).

[324] R.C. Buck, P.M. Murphy, M. Pabon, in: 2012, pp. 1–24.

[325] H.-J. Lehmler, Chemosphere 58 (2005) 1471–1496.

[326] A. Zaggia, B. Ameduri, Curr Opin Colloid Interface Sci 17 (2012) 188–195.